A WEST Wind Climate Simulation of the Mountainous Yukon

J. D. Jean-Paul Pinard[1*], Robert Benoit[2] and Wei Yu[2]

[1]*University of Alberta, Edmonton AB*
[2]*Recherche en Prévision Numérique (RPN), MSC, Environment Canada, Dorval PQ*

[Original manuscript received 8 October 2004; in revised form 5 April 2005]

ABSTRACT *The wind climate of the mountainous terrain in the southern Yukon is simulated using the Wind Energy Simulation Toolkit (WEST) developed by the Recherche en Prévision Numérique (RPN) group of Environment Canada and is compared to measurements in the field. WEST combines two models that operate at different spatial scales. The Mesoscale Compressible Community (MC2) model is a mesoscale numerical weather prediction model that produces simulations over large domains of the order of a thousand kilometres. The MC2 model uses long-term synoptic scale wind climate data from the analysis of radiosonde and other observations to simulate mean wind fields at tens of metres above the ground using a horizontal resolution of a few kilometres. The mesoscale results are used as input to MS-Micro/3 (Mason and Sykes (1979) version of the Jackson and Hunt (1975) model version for microcomputers/3-dimensional; MS-Micro hereafter), a more computer-efficient, microscale model with simpler linearized momentum equations and a domain restricted to a few tens of kilometres with horizontal grid sizes of tens or hundreds of metres. MS-Micro provides wind field results at specific wind generator hub heights (typically 30 to 50 m above ground level (AGL)) which are of interest to researchers and developers of wind farms.*

WEST shows relatively strong correlations between its simulated long-term mean wind speed and the measurements from ten wind energy monitoring stations. However, in the mountainous terrain of the Yukon, WEST tends to predict wind speeds which are about 40% too high. The model also produces erroneous wind directions and some were perpendicular to valley orientations. The most likely cause of the wind speed and direction errors is the substantially modified 5-km grid-spaced mesoscale terrain used in MC2. The WEST simulation was also found to double the wind speeds observed at airport stations and there was poor correlation between the simulated and observed wind speeds.

The bias in the model could be attributed to a number of factors, including the use of smoothed topography by the model, the discrepancy between the neutral atmosphere assumed in MS-Micro and the normally observed stable atmosphere, the application of MS-Micro to every third grid point of the MC2 output, abnormally high sea level wind speeds in the input climate data for MC2, and a certain degree of disagreement between the land surface characteristics used in the model and those found in the field.

At comparatively low computer cost, WEST predicts a wind climate map that compares favourably to the wind measurements made in several locations in the Yukon. However, the problem of the modified terrain in the mountainous regions is the most pressing problem and needs to be addressed before WEST is used in the mountainous regions of Canada.

RESUMÉ *[Traduit par la rédaction] On simule le climat du vent dans la partie montagneuse du sud du Yukon à l'aide du Wind Energy Simulation Toolkit (WEST) mis au point par le groupe de Recherche en prévision numérique (RPN) d'Environnement Canada et on le compare aux mesures faites sur le terrain. Le WEST combine deux modèles fonctionnant à des échelles spatiales différentes. Le modèle de mésoéchelle compressible communautaire (MC2) est un modèle de prévision numérique de mésoéchelle qui produit des simulations dans de grands domaines de l'ordre du millier de kilomètres. Le modèle MC2 utilise des données climatologiques sur le vent à l'échelle synoptique à long terme provenant de l'analyse de radiosondage et d'autres observations pour simuler les champs de vent moyen à quelques dizaines de mètres au-dessus du sol avec une résolution horizontale de quelques kilomètres. Les résultats à mésoéchelle sont utilisés comme entrées dans le MS-Micro/3 (la version Mason et Sykes (1979) de la version du modèle de Jackson et Hunt (1975) pour micro-ordinateurs/tridimensionnel; MS-Micro ci-après), un modèle de microéchelle mieux adapté aux ordinateurs avec des équations de quantité de mouvement linéarisée plus simples et un domaine limité à quelques dizaines de kilomètres découpé par une grille horizontale de quelques dizaines ou quelques centaines de mètres. MS-Micro/3 fournit des résultats de champs de vent aux hauteurs où se retrouvent typiquement les moyeux d'éoliennes (en général de 30 à 50 m au-dessus du sol) et qui présentent un intérêt pour les chercheurs et les promoteurs de parcs d'éoliennes.*

WEST montre des corrélations assez fortes entre ses simulations à long terme de la vitesse moyenne du vent et les mesures faites à dix stations mesurement d'énergie éolienne. Cependant, dans la région montagneuse du Yukon, WEST a tendance à prédire des vitesses de vent environ 40 % trop élevées. Le modèle produit aussi des

*Corresponding author's e-mail: jppinard@polarcom.com; current address-703 Wheeler St., Whitehorse YT Y1A 2P6

directions de vent erronées et certaines étaient perpendiculaires à l'orientation des vallées. La cause la plus probable des erreurs de vitesse et de direction du vent est la représentation à mésoéchelle du terrain (modifié de façon importante) avec un pas de grille de 5 km utilisée dans MC2. On a aussi trouvé que la simulation WEST doublait les vitesses de vent observées aux stations aéroportuaires et la corrélation était mauvaise entre les vitesses simulées et les vitesses observées du vent.

On peut attribuer le biais dans le modèle à différents facteurs, y compris l'utilisation d'une topographie lissée par le modèle, l'écart entre l'atmosphère neutre supposée dans MS-Micro et l'atmosphère stable normalement observée, l'application de MS-Micro à tous les trois points de grille de la sortie de MC2, les vitesses de vent au niveau de la mer anormalement élevées dans les données climatologiques d'entrée de MC2 et un certain degré de désaccord entre les caractéristiques de la surface terrestre utilisées dans le modèle et celles que l'on observe sur le terrain.

Pour un coût en ordinateur comparativement bas, WEST prédit une carte climatologique du vent se comparant favorablement aux mesures de vent faites à plusieurs endroits au Yukon. Cependant, le problème du terrain modifié dans les régions montagneuses est le problème le plus important et il faut s'en occuper avant que WEST soit utilisé dans les régions montagneuses du Canada.

1 Introduction

Wind farms are the fastest growing energy sector in the world today. With this new development has come the need for greater accuracy in mapping the wind climate near the ground in order to allow wind farm developers to identify areas of high wind energy potential.

Wind maps have been produced for Europe (Troen and Petersen, 1989), the United States (Elliot and Schwartz, 1993), and other parts of the world. In Canada, Walmsley and Morris (1992) made the first attempt at defining the country's wind climate. Their map was an interpolation based on wind data from 144 weather observation sites across the country, four of which were in the valleys of the Yukon. The map provided some clues to windy areas but failed to show realistic winds in the mountainous regions of British Columbia and the Yukon Territory. The next Canadian wind mapping attempt was by Benoit et al. (2001) (Vincent, 2001; National Geographic, 2002) who used Canadian Meteorological Centre (CMC) operational forecasts computed with grid spacing of 24 km and averaged over five years (1996–2000). This map was still relatively coarse, especially from an orographic perspective, and indicated that the Yukon wind regime was still not adequate for cost-effective power production even though independent observations showed otherwise. Subsequent model runs, however, by Benoit et al. (2001) at a grid spacing of 5 km compared better with field measurements for the Gaspé region than those from the 24-km forecasts, presumably due to better resolution of terrain.

New modelling techniques have recently been employed with some degree of success in simulating the wind climate using a combined mesoscale-microscale model. Frank et al. (1999) experimented with the Karlsruhe Atmospheric Mesoscale Model (Adrian and Fiedler, 1991) and the microscale Wind Atlas Analysis and Application Program (WAsP) (Mortensen et al., 1993) in Finland. Brower et al. (2004) used the Fifth-Generation NCAR/Penn State Mesoscale Model (MM5) and a mass consistent model for the microscale in a number of different climatic regions.

The Wind Energy Simulating Toolkit (WEST) uses the Mesoscale Compressible Community (MC2) model (Benoit et al., 1997) and the linearized microscale model MS-Micro/3 (Mason and Sykes (1979) version of the Jackson and Hunt (1975) model version for microcomputers/3-dimensional; MS-Micro hereafter) (Walmsley et al., 1990) to produce wind maps of large regions. The WEST has been successfully used to simulate the wind energy potential for several regions across Canada and other parts of the world and it is also being applied to compute a unified wind atlas (see www.windatlas.ca) for the entire country. Whereas most of Canada has relatively low relief terrain, the British Columbia-Yukon region is very mountainous and presents a challenge to models whose grid spacing is relatively coarse compared to the spatial variation of the mountainous terrain of the Yukon. In this region many mountain ridges are too narrow to be completely resolved in a 5-km model grid. WEST, with the inclusion of MS-Micro, provides modelling capabilities to grid sizes of a few hundred metres.

In this paper we use WEST to simulate the wind climate of the southern Yukon and compare its output to field measurements. We describe the orography and wind climate of the territory in Section 2. The field measurements, their surrounding land use, and the variability and vertical projection errors are discussed in Section 3. The toolkit structure is described in Section 4. The simulation domain with the climate and surface inputs are described in Section 5. Although the purpose of WEST is to make use of MS-Micro to refine the MC2 output of wind values near complex surfaces, the outputs of both models are examined and compared in Section 6 and a discussion follows in Section 7.

2 Orography and wind climate of the southern Yukon

A map of the Yukon is given in Fig. 1 and shows the major mountainous features in and around the territory. Most of the communities in the territory are below 1000 m (heights are given above sea level (ASL) unless otherwise stated). The thicker 2000-m contour lines indicate some of the higher mountainous regions in the territory. It can be observed that the Wrangell-St. Elias Mountains are rather extensive and dominate the south-west Yukon with several peaks above 3000 m. This range also contains Canada's highest peak, Mount Logan, with a height of 5959 m.

To the north-east of the St. Elias Mountains is the Yukon Plateau, which makes up the southern two-thirds of the territory. The name "plateau" is a misnomer, since this area, which ranges

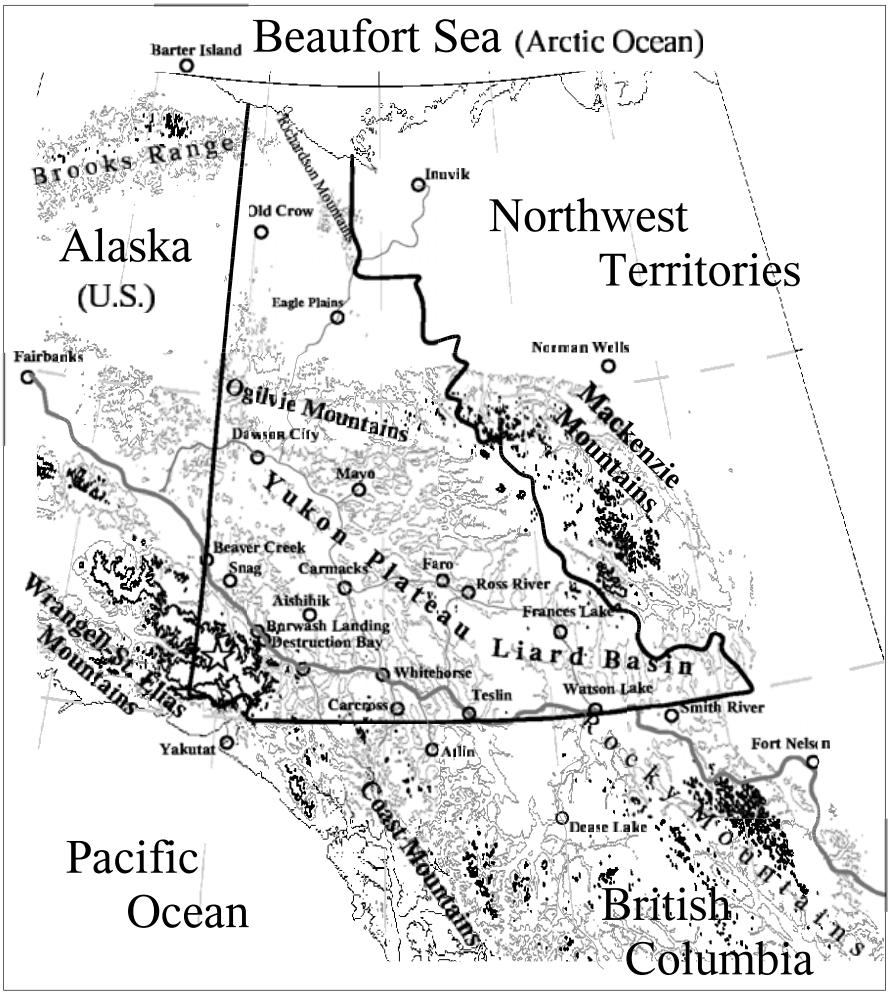

Fig. 1 This map shows orographic features in and around the Yukon. The thin contour line is at 1000 m ASL and the thicker contour is at 2000 m ASL. The Wrangell-St. Elias Mountains are shown to be the largest and highest mountain range in the Yukon Territory. Its highest peak is Mt. Logan at 5959 m ASL (star symbol in south-west Yukon).

from about 300 m to about 2000 m, is not particularly flat. The plateau is bordered to the north-east by the Mackenzie Mountains and to the north by the Ogilvie Mountains. The valleys and ridges are generally oriented in a south-east to north-west direction. This region is home to more than 95% of the territory's population, and includes Whitehorse, Watson Lake, Dawson City, Haines Junction and a number of smaller communities.

The territory's wind climate is highly influenced by its mountainous terrain. Whitehorse, for example, is located in a north-north-west to south-south-east oriented valley about 200 km north of the Pacific Coast. Analysis of upper air and surface wind data shows that the prevailing wind in the Whitehorse valley is mostly from the south-south-east, restricted by the valley orientation. Above the nearby mountaintops, the prevailing wind direction is less constrained and tends to be from the south-west to west. Similar low level conditions are found in the Kluane Lake region (Shakwak Trench; see Fig. 2) and Faro (Tintina Trench) where prevailing winds are from the south-east and follow the valleys.

Mountaintop winds are stronger in the winter than in the summer, whereas in the valleys the opposite is generally true; the summer valley winds are stronger than those in winter. The upper winds in winter seem to have less influence on the colder, slower-moving air masses in the valleys. Data from the Whitehorse radiosonde station show that a much stronger vertical wind shear exists during the winter than during the summer. This seasonal variation in the vertical wind shear presents difficulties in correlating mean annual winds between wind stations at different elevations.

3 Wind monitoring sites in the territory

The locations of the wind monitoring stations used in this study are shown in Fig. 2. The stations are listed in Table 1 and are classified as an "airport" station or a "wind energy" station. There are seven airport stations, indicated with an "A" in the figure, that were established for airport weather monitoring. The compiled wind data for the airport stations originate from the Atmospheric Environment Service (AES)

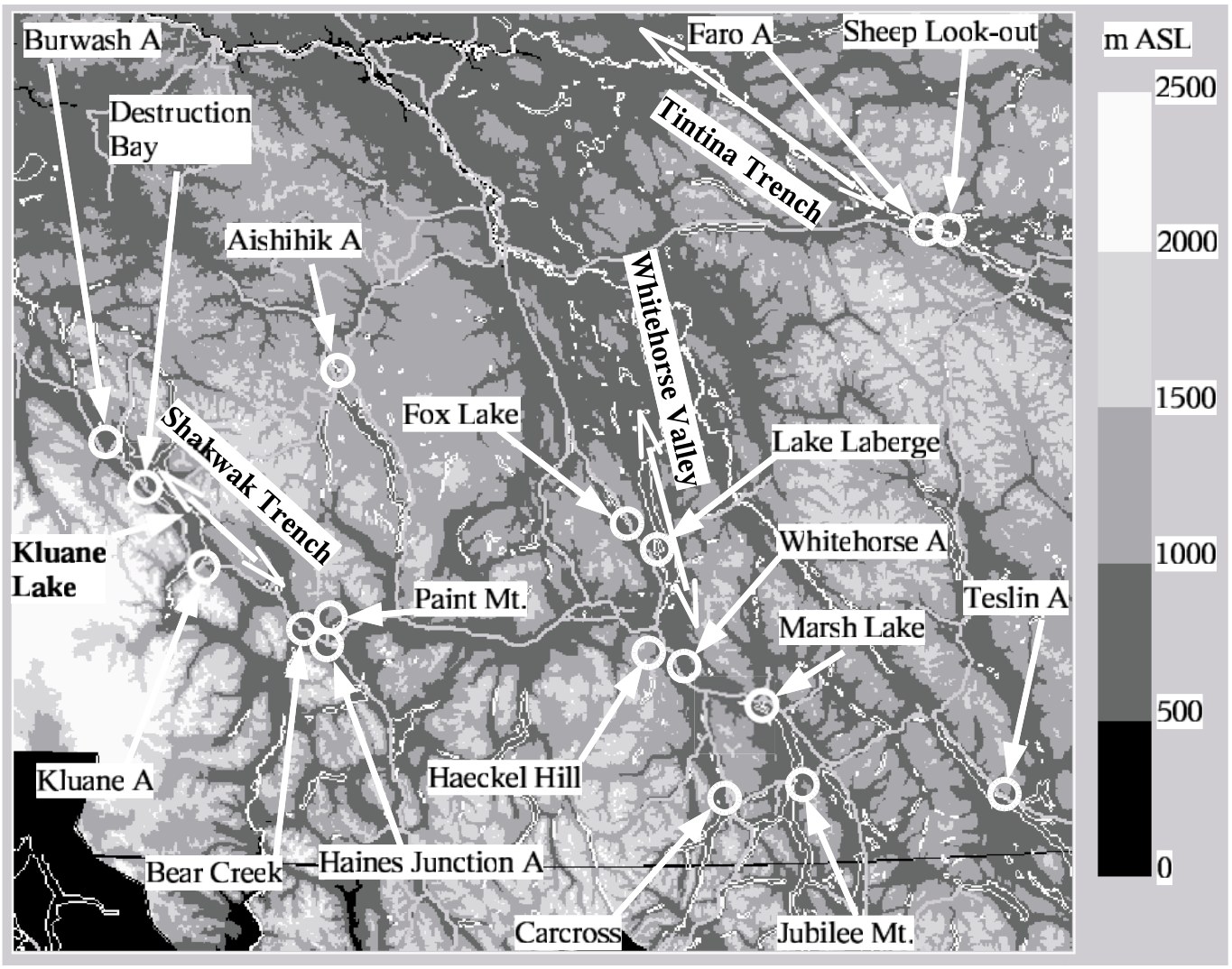

Fig. 2 Map of the southern Yukon showing the airport and the wind energy stations overlaid on the microscale map used for the MS-Micro simulations. The values in the legend are elevations in metres ASL. The white lines are major rivers and lakes and the thicker grey lines are highways and secondary roads. Note that most of the stations are in the valleys; the three exceptions are Paint Mountain, Jubilee Mountain and Haeckel Hill.

(AES,1982) and span five years or more (columns 4 and 5, Table 1). The wind sensors were mounted at approximately 10 m above ground level (AGL) (column 3, Table 1) and most of the stations were located near airports. Aishihik, Teslin, Haines Junction, and Whitehorse were 24-hour observation sites, whereas Faro and Burwash were daytime hourly. The frequency of wind observations at Kluane was not known. The method of recording wind information has been by human observation of a dial for both the wind speed and direction, subjectively averaged over two minutes. More detailed information can be found in Weather Services Directorate (1977) and AES (1976).

The Teslin, Faro, and Burwash stations were located in open fields within a few hundred metres of their respective terminal buildings. The Haines Junction station was in an open pasture in a low-lying depression surrounded by small forested hills. It is possible that buildings and nearby trees may have had diminishing effects on the wind speed at these wind stations. The Kluane and the Aishihik stations were dismantled and their exact locations and the surrounding surface roughness conditions are uncertain. The Whitehorse weather station is the most exposed of the airport group. It is located in a short-grass field on a high bank above the city of Whitehorse and clearly open to both the occasional north-north-west wind and the dominant south-south-east wind. The station is about 500 m east of the airport buildings. Observed and best estimates of surface roughness for all these stations are listed in column 7 of Table 1 and also in Table 3, which is discussed in Section 5c.

The “wind energy” group consisted of ten wind stations with sensors at heights ranging from 10 to 30 m AGL (column 3, Table 1). For each station, the wind fields were sampled every one or two seconds and the mean statistics were recorded every 10 minutes. The following stations ran for one year: Fox Lake (Cottrell-Tribes, 2002a), Carcross (Cottrell-Tribes, 2002c), Lake Laberge (Cottrell-Tribes, 2002b), Marsh

TABLE 1. List of the wind stations used for the model comparison. The heights of the station surfaces and the sensor towers are shown in columns (2) and (3). The period of monitoring and duration are in columns (4) and (5) and the mean wind speeds for the period are in column (6). The surface roughness used to project the wind speeds from their measured heights to 30 m are listed in column (7) and are also referred to in Table 3. The projection of the wind speeds from the measured heights to 30 m are listed in columns (8) and (9) and are calculated using Eq. (1) and the roughness lengths (column 7) for each station. This projection implies possible errors which are shown in columns (10) to (13). There are also errors due to the possible variability of a short monitoring period length to long-term mean in which these stations measured. These errors are shown in columns (14) and (15). Columns (16) and (17) are the total errors that may exist in the measurements. The values in columns (9), (16) and (17) are emboldened; they are compared to the WEST simulation and are also shown graphically in Fig. 12 along with the model results. Other possible errors used here are sensor and data logger errors which are apparently small enough to be insignificant in this analysis.

Column (1)	(2)	(3)	(4)	(5)	(6)	(7)	(8)	(9)	(10)	(11)	(12)	(13)	(14)	(15)	(16)	(17)
	Heights		Monitoring				Projection		Projection Error to 30 m				Period Error		Total errors	
	ASL	Tower AGL	Period	Duration	Mean wind speed	Surface Roughness length	Ratio to 30 m	Speed at 30 m	Ratio	Below mean	Ratio	Above mean	Error	30-m Speed	Below mean	Above mean
	(m)	(m)	(year)	(years)	(m s^{-1})	(m)		(m s^{-1})	Min	(m s^{-1})	Max	(m s^{-1})	(%)	(m s^{-1})	(m s^{-1})	(m s^{-1})
Airport																
Aishihik A	966	10	1944–66	12	2.8	0.05	1.21	**3.3**	1.14	-0.2	1.35	0.4	0.06	± 0.2	**-0.4**	**0.6**
Burwash A	799	10	1966–80	14	3.4	0.10	1.24	**4.2**	1.14	-0.3	1.35	0.4	0.06	± 0.3	**-0.6**	**0.6**
Faro A	694	10	1972–77	5	2.1	0.10	1.24	**2.7**	1.14	-0.2	1.35	0.2	0.06	± 0.2	**-0.4**	**0.4**
Haines Junction A	599	10	1963–80	15	1.8	0.20	1.28	**2.3**	1.14	-0.3	1.35	0.1	0.06	± 0.1	**-0.4**	**0.3**
Kluane Lake A	786	10	1974–80	5	2.5	0.05	1.21	**3.0**	1.14	-0.2	1.35	0.4	0.06	± 0.2	**-0.3**	**0.5**
Teslin A	705	10	1955–80	20	2.2	0.20	1.28	**2.8**	1.14	-0.3	1.35	0.2	0.06	± 0.2	**-0.5**	**0.3**
Whitehorse A	703	10	1955–80	26	3.6	0.02	1.18	**4.2**	1.14	-0.1	1.35	0.6	0.06	± 0.3	**-0.4**	**0.9**
Wind Energy																
Sheep Look-out, Faro	795	30	2000–02	2	4.6	1.00	1.00	**4.6**	1.00	0.0	1.00	0.0	0.12	± 0.6	**-0.6**	**0.6**
Haeckel Hill	1440	30	1998–01	2	7.1	0.01	1.00	**7.1**	1.00	0.0	1.00	0.0	0.06	± 0.4	**-0.4**	**0.4**
Destruction Bay	823	30	1995–98	3	6.0	0.05	1.00	**6.0**	1.00	0.0	1.00	0.0	0.06	± 0.4	**-0.4**	**0.4**
Bear Creek	670	26	1998–00	2	4.9	0.01	1.02	**5.0**	1.00	-0.1	1.06	0.2	0.06	± 0.3	**-0.4**	**0.5**
Fox Lake	793	20	2001–02	1	2.2	3.85	1.25	**2.7**	1.05	-0.4	1.31	0.1	0.14	± 0.4	**-0.8**	**0.5**
Carcross	702	20	2001–02	1	3.3	3.55	1.23	**4.1**	1.05	-0.6	1.30	0.2	0.14	± 0.6	**-1.2**	**0.8**
Lake Laberge	645	10	2001–02	1	3.8	0.01	1.16	**4.5**	1.14	-0.1	1.35	0.7	0.14	± 0.6	**-0.7**	**1.4**
Marsh Lake	656	10	2000–01	1	2.6	0.01	1.16	**3.0**	1.14	-0.1	1.35	0.5	0.14	± 0.4	**-0.5**	**0.9**
Paint Mountain	1370	10	1992–94	2	4.4	0.05	1.21	**5.3**	1.14	-0.3	1.35	0.6	0.12	± 0.6	**-0.9**	**1.3**
Jubilee Mountain	1280	10	1993–94	1	3.5	0.05	1.21	**4.3**	1.14	-0.2	1.35	0.5	0.14	± 0.6	**-0.8**	**1.1**

Lake (Cottrell-Tribes, 2001), and Jubilee Mountain (Baker, 1995). Sheep Look-out (Cottrell-Tribes, 2003), Haeckel Hill (Cottrell-Tribes, 2000b), Bear Creek (Pinard, 2001) and Paint Mountain (Baker, 1995) operated for two years. Destruction Bay (Cottrell-Tribes, 2000a) operated for three years.

The sites for wind energy stations were normally chosen in order to have maximum exposure to the prevailing winds. The stations at Haeckel Hill (30 m AGL), Paint Mountain (10 m AGL), and Jubilee Mountain (10 m AGL) were located on mountaintops with surfaces of bare rock and low shrubs. Sheep Look-out (30 m AGL) was in an approximately 8-m tall poplar forest on a small hill in the valley of the Tintina Trench open to the south-east winds. The Lake Laberge (10 m AGL) site was on a small smooth-rocked hill by the lake shore which was exposed to dominant south-east winds. Destruction Bay (30 m AGL) was located on a grassy bank along the Kluane Lake shoreline and open to the prevailing south-east winds. Bear Creek (26 m AGL) was also on a short-grassed bank and open to frequent winds of the Alsek Valley to the south-east. The Carcross station (20 m AGL) was in a 6-m tall poplar forest on a hill exposed to winds from Bennett Lake to the south-west. The Marsh Lake station (10 m AGL) was on a sandy beach and open to the lake to the south and south-east. Fox Lake (20 m AGL) station was located in an area of heavily wooded spruce trees approximately 15 m high in a north-north-west to south-south-east valley. More details on their surface roughnesses can be found in Table 3.

In order to project the short monitoring periods of a wind energy station to long-term means, correlations of monthly mean wind speeds have been computed between three of the stations and nearby airport stations. Destruction Bay was shown (Cottrell-Tribes, 2000a) to have a correlation of R = 0.91 with the Burwash airport station, its mean speed was projected to a 30-year long-term mean and is noted in column 6 of Table 1. The Bear Creek station had a correlation of about 0.85 with the nearby Haines Junction station, its mean wind was projected to 12 years. Haeckel Hill had a correlation coefficient of 0.93 to the nearby upper air data interpolated at 1400 m and was projected to nine years. Errors due to the variability from the long-term mean at these stations are addressed in the next paragraph.

The other stations correlated poorly with their nearest long-term neighbour, and as a result, the possible error due to the variability in the shorter monitoring periods is examined by analysing long-term data available for the Whitehorse and Haines Junction airport stations. These two stations had very similar results. The Whitehorse station, which has the longer period of record, is shown in Fig. 3. The data used here are monthly mean wind speeds from a 10-m tower for the period 1990 to 2004. Figure 3 shows the minimum, maximum, and the standard deviations of the mean wind speed for five different running average periods over the long-term monthly mean of the dataset. The values in the figure show that the mean wind speed for a wind monitoring period of less than one year will likely vary more than ±14% from the long-term mean. For a two-year monitoring period we would expect the mean to vary less than ±12% from the long-term mean. The variability diminishes further for the three- and five-year means to ±9% and ±6% respectively. This analysis suggests that the mean wind speeds for all of the airport stations should not vary by more than 6% from the long-term mean since their record lengths are five years and longer. The variations for these stations are shown in columns 14 and 15 of Table 1. Using the above argument, we assume that those wind energy stations that correlated with the long-term stations probably had maximum variability errors of about 6%. One could argue that the error might be closer to 12% because these stations collected data for two years or more and that the correlation might not be representative. Consequently, this translates to a wind speed error, say for a 6-m s^{-1} wind speed, of 0.7 m s^{-1} at 12% and 0.4 m s^{-1} at 6% error.

All comparisons in this study were made at a height of 30 m AGL, a typical hub height for community scale wind turbines. (MS-Micro is capable of producing results at any specified height, but only 30 m was chosen for this study.) The measured wind speeds below 30 m AGL and the MC2 wind speed at 65 m AGL were projected vertically to 30 m AGL using a simple logarithmic profile that makes use of the surface roughness z_0 for each site, namely

$$\overline{u}\left(z_p\right) = \overline{u}\left(z_m\right)\frac{\ln\left(z_p \,/\, z_0\right)}{\ln\left(z_m \,/\, z_0\right)} \qquad (1)$$

where the wind speed $\overline{u}(z_m)$ measured (or modelled) at height z_m is projected vertically to a new speed $\overline{u}(z_p)$ and height z_p.

This logarithmic projection was performed instead of obtaining the wind speeds directly from the model for the exact heights at which the measurements were taken. At the time the modelling was done, results could not be obtained for 10 m or 20 m. For MC2, because of model stability and computer resources, it has been problematic to use a near-surface grid spacing smaller than 65 m in the vertical.

The vertical projections may seem to impair the purpose of this model-to-measurement comparison. The simple logarithmic projection of wind speed may not be accurate in complex terrain with varying surface heights and roughnesses. This relation also assumes neutral stratification which will reduce the differences between the projected wind speeds between two heights. However, at this relatively early stage of the WEST model development it may not be critical considering that a 65-m high point in the MC2 model represents a 5-km square area. It will become more evident in Section 6 that the errors in the vertical projection will not significantly impede the model-to-measurement comparison. The more important analysis and discussion will be in the bias between the model and the measurements that are likely more related to the model terrain. In a future study MS-Micro will be configured to produce wind speeds at 10-m heights in order to avoid the problem of vertical projections.

Using Eq. (1) the vertical projection ratios were calculated for each station and are shown in column 8 of Table 1 with

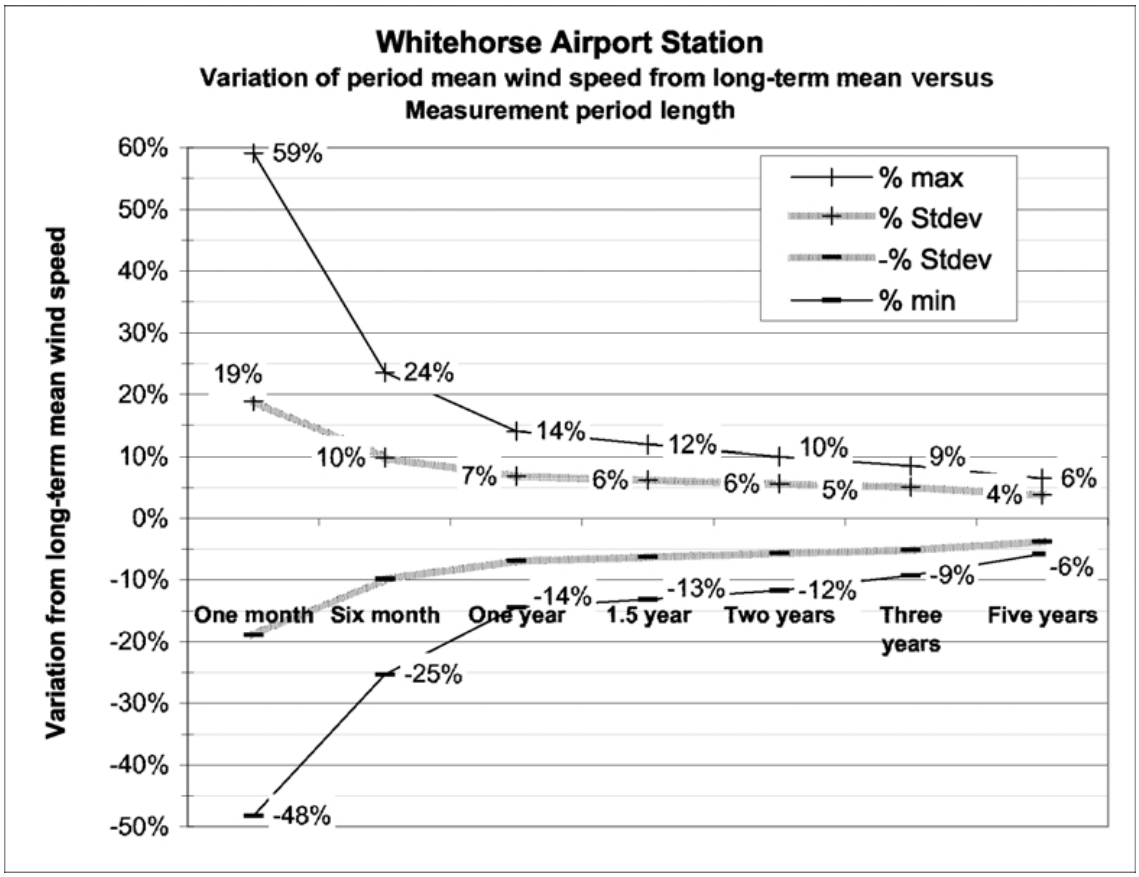

Fig. 3 This graph compares the variability of different period lengths of a running average to the long-term mean for the Whitehorse airport station. The analysis is from monthly mean wind speeds (at 10 m ASL) for the years 1990 to 2004. The standard deviations, minima, and maxima of running means for different period lengths are displayed. The minimum and maximum percentage values are used in the analysis, the standard deviations are for comparative purposes only.

their corresponding new wind speeds at 30 m AGL in column 9. Taking into account that projecting wind speeds vertically also results in errors, a calculation of possible minimum and maximum projection ratios was made. The smallest wind speed increase from, say 10 m to a height of 30 m could be computed from Eq. (1) using the smoothest surface that could exist at a site, that is, a value of z_o = 0.003 m, for the surface roughness of a flat short-grass field. At the 30-m height this results in a speed increase of 1.14 times the 10-m speed value and is correspondingly smaller for the 20-m heights. The Bear Creek station at 26 m was chosen to have no increase as a low estimate. These values are listed in column 10 and the wind speed differences between the calculated mean and the minimum (negative signs) are shown in column 11 of Table 1. The maximum possible increase for the 10- to 30-m heights is inferred from a compilation of mean wind speed profiles from various 30-m stations in the territory and particularly from analysis of the Whitehorse upper air station. These profiles show that, for the normally stable atmosphere and typical surface roughness in Yukon valleys, the maximum increase in speed from 10 to 30 m is about 1.35 times. The speed projections from the other heights, 20 m and 26 m, are made using a logarithmic interpolation scheme that fits the vertical profiles of the measurements. These projection values, along with the mean to maximum speed differences at 30 m, are listed in columns 12 and 13 of Table 1.

The total wind speed projection errors due to the vertical projections and the variability in the temporal means are listed in columns 16 and 17 of Table 1. Other possible sources of error are the sensors and the data recording devices. These errors are assumed to be small and are not considered in the analysis.

4 WEST: the wind energy simulation toolkit

This section briefly describes the toolkit and the MC2 and MS-Micro models. WEST combines the mesoscale model MC2 (Benoit et al., 1997) and the microscale model MS-Micro (Walmsley et al., 1990) to produce a wind map of a large complex region of interest. The reason for the two-model combination in WEST is that the formulation of MS-Micro is much simpler (Jackson and Hunt, 1975) than that of MC2. The problem with reducing the MC2 grid spacing to, say below 1 km (horizontal), is that it requires greatly increased computer resources to deal with the exponentially

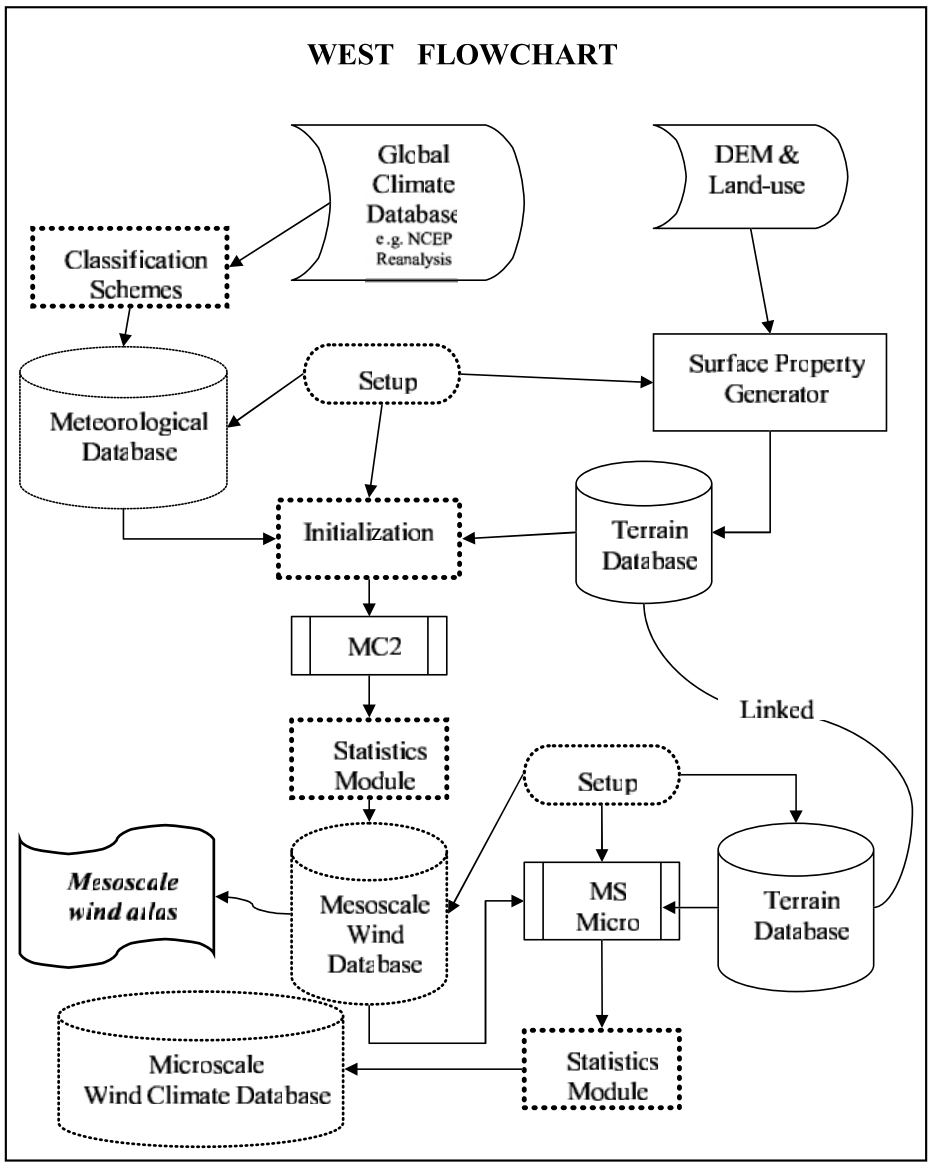

Fig. 4 The WEST flowchart includes four important modules: a classification scheme for the climate data, the MC2 mesoscale modelling engine, a statistics module, and a microscale modelling engine. The meteorological database is derived from the NCEP/NCAR reanalysis. The DEM and land use data are from the USGS database.

increased number of grid points. MS-Micro helps to reduce the final grid spacing to several tens of metres without significantly increasing processor time. With MS-Micro, only the target heights (say, a wind turbine hub height of 30 m AGL) need to be computed, resulting in an efficient two-dimensional microscale flow model.

The structure of the toolkit is shown in Fig. 4. For initialization, WEST includes a dataset of wind climate statistics (described in Section 5a) generated through a classification scheme that is available in a meteorological database. The digital elevation model (DEM) and the surface roughness (land use; described in Section 5c) are also taken into account using a surface property generator. These are available in a terrain database for use by both MC2 and MS-Micro. Through the initialization scheme, these databases are used by MC2. The output of MC2 is post-processed with a statistics module and stored in a mesoscale wind database. This database is useful for analysing mesoscale wind fields and has been used for Environment Canada's wind atlas (see www.windatlas.ca). In WEST, the mesoscale wind database is used by the microscale model, MS-Micro, along with the terrain data generated from a higher resolution terrain database with the same algorithm used for MC2. There is a mesoscale-microscale coupling scheme that consists of multiple microscale domains centred on each mesoscale grid point (or every third point in WEST, more details are given in Section 5d). The microscale domains overlap each other and a blending scheme is applied to combine each domain into one single large grid covering the entire mesoscale domain. There can be one to ten thousand such microscale domains executed in a single mesoscale domain.

The statistics module is applied to the MS-Micro output and the data are stored in a microscale wind database. Both the mesoscale and the microscale data can be sent to a post-analysis graphical package for viewing and analysis.

a *MC2*

The MC2 model has been developed over several years by the Recherche en Prévision Numérique (RPN) group in Dorval, Québec. MC2 is a limited area model with a terrain-following vertical coordinate system, open boundaries, and self-nesting capabilities. It is non-hydrostatic, three-dimensional, time dependent, with fully compressible Navier-Stokes equations. The model has a semi-implicit formulation with a stationary isothermal hydrostatic basic state, and a three-dimensional semi-Langrangian advection. The complete formulation of the model dynamics can be found in Tanguay et al. (1990) and Benoit et al. (1997).

MC2 can be run in two configurations, one being a weather forecast mode where time is critically important and all of the "physics" in the model are used. The second mode, which is used in the present study, is time independent and is more of a boundary-layer type flow where the lower 5 km AGL are most important. Here most of the "physics" are not used, the initial state is simplified, that is, the isobars are straight at all levels, and the model is allowed to achieve pseudo-equilibrium. The only physics component invoked is the adiabatic turbulent boundary layer.

The turbulence closure scheme used for this model is described in Mailhot et al. (1998). It is based on a vertical diffusivity formulated as the product of the square root of the turbulent kinetic energy and a length scale that is proportional to height. The product of these two terms is divided by a static stability function dependant on the Richardson number. The vertical diffusion coefficient, consequently, is variable throughout the model layers and should reflect the intensity of the turbulent exchanges near the surface. At the surface, the turbulent fluxes are continuous with surface energy exchanges computed from Monin-Obukhov similarity theory. At the upper boundary, the flux vanishes.

b *MS-Micro*

Jackson and Hunt (1975) developed a linearized dynamical model for turbulent flow over a shallow two-dimensional hill. Mason and Sykes (1979) took their two-dimensional formulation and extended it to three dimensions. This development led to the creation of MS-Micro and of WAsP (Troen and Petersen, 1989).

MS-Micro (Walmsley et al., 1990; Walmsley et al., 1982; Taylor et al., 1983; Walmsley et al., 1986) consists of a vertical coordinate system that follows the terrain of a gently sloped hill whose shape and size define scaling parameters and are, in principle, compatible with the linearization of equations of motion.

The model assumes a neutrally stratified atmosphere that consists of an inner and an outer layer. The outer layer is represented by pressure gradients determined by an inviscid and irrotational potential flow. The outer solution provides the perturbation pressure fields that force the elevation-induced flow perturbations within the inner layer.

The momentum budget of the inner layer is a balance between advective, pressure-gradient, and turbulent-viscous forces in the form of linearized perturbation momentum equations. The turbulent transfers are parametrized by a simple mixing length closure scheme. The velocity perturbations of governing equations are solved analytically with the use of Finite Fourier Transforms. These transforms impose limitations on the model circumstances and may reduce the accuracy of the solutions. The most important of these limitations is that neutral stratification is assumed, others are that the slopes must be less than 25%, and the Coriolis force is neglected. The suggested size of the model is to be no more than 10 km (size of the "island", see Section 5d) and that the vertical solution levels are within 1 to 150 m AGL.

5 Inputs and settings for the southern Yukon simulation

A model simulating a real life situation is only as good as the data that are available to it. In this section we attempt to ensure that the input data represent the reality that is being simulated. In Section 5a we describe the climate data that are used in the mesoscale model MC2. In Section 5b we compare the input climate data with the upper air data from Whitehorse and to some extent, Yakutat. In Section 5c the land use data and the DEM are also examined and compared to observations at the monitoring sites. Section 5d provides a description of the model configuration and some of the methods which were used when the combined simulations in WEST were carried out for the southern Yukon case.

a *The MC2 Input Climate Data*

Meteorological centres, such as the Canadian Meteorological Centre, the National Centers for Environmental Prediction (NCEP), and the European Centre for Medium-range Weather Forecasts collect and analyse data from surface stations, radiosondes, ships, airplanes, radars, and satellites every six hours. These centres are able to provide long series of quality controlled and analysed three dimensional (3-D) global data grids. Subsets of theses data for the region of interest, serve as the input to the MC2 model, used in the Yukon wind simulation with WEST.

The wind climate classification follows the methodology set out in Frank and Landberg (1997). Each element of the time series of the geostrophic wind (components u_g in the east direction, v_g in the north direction) at 1000 mbar (near sea level) during the 44 years of NCEP Reanalysis data (Kalnay et al., 1996) is classified into tri-variate bins for

(a) direction (16 bins),
(b) speed (3–7 bins, depending on overall frequency of occurrence for that direction), and
(c) 1000–850 mbar geostrophic shear (2 bins, i.e., positive and negative shear).

The overall number of possible bins is $16 \times 7 \times 2 = 228$. The actual number of non-empty bins is climate dependent for

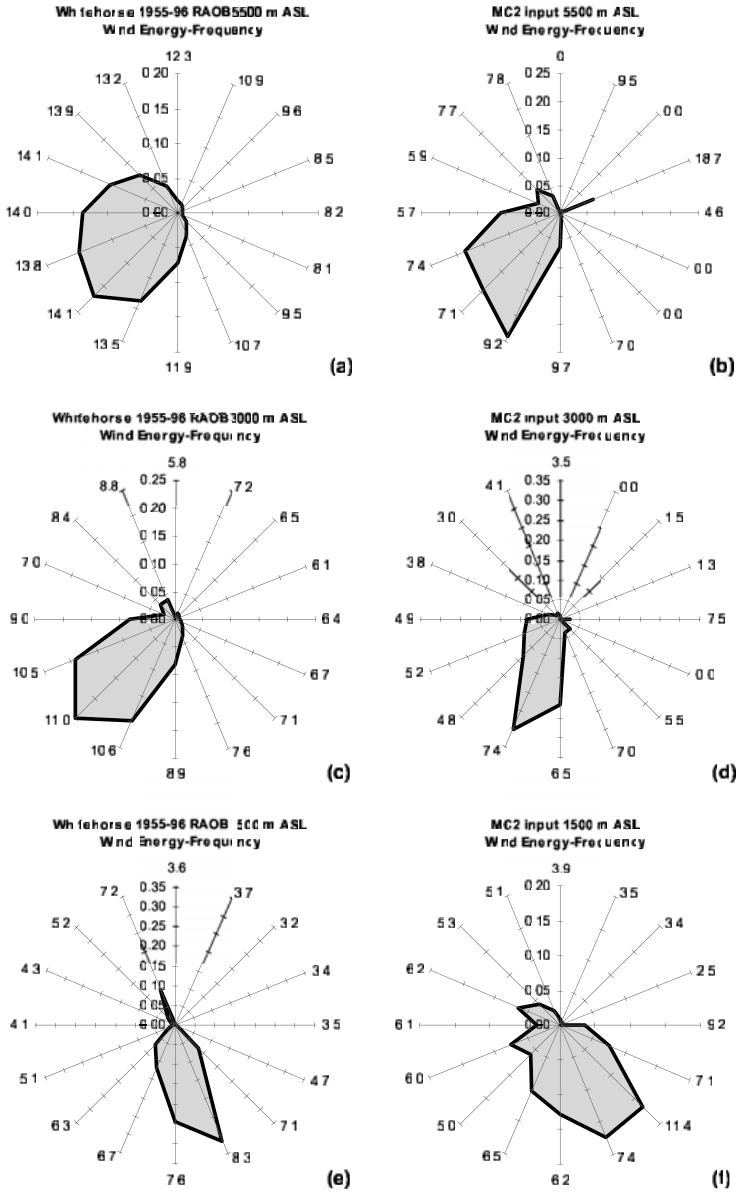

Fig. 5 Wind energy-frequency roses for the Whitehorse upper air station on the left and the MC2 input data on the right, are shown at three elevations: 5500, 3000, and 1500 m. The wind energy-frequency rose is calculated, for each direction, as the product of the cube of the mean wind speed and its frequency of occurrence divided by the sum of those products in all directions. The long-term mean annual wind speed that occurs in each of the 16 directions is labelled at the end of each arm. The roses show that the wind climate input data for MC2 compares reasonably well with the Whitehorse data in terms of direction but displays rather low wind speeds at the 3000 and 5500 m levels.

each region and for the southern Yukon there are 162 bins. The wind speeds and directions from these bins were compiled and are presented in the form of wind energy-frequency roses in Fig. 5 and Fig. 6. These are discussed in Section 5b.

For each climate bin one MC2 run is executed, thus 162 runs are made for the southern Yukon. The whole 3-D mesoscale grid is initialized from the data of each bin component, that is, that bin's set of values for u_g, v_g, and temperature at four levels, 0, 1500, 3000, and 5500 m. This is a level-by-level geostrophic-hydrostatic initialization scheme that initializes the model fields to a horizontally uniform state (as seen along iso-planes of the vertical coordinate). It amounts to spreading the single profile for that bin, or climate condition, to the entire 3-D grid according to simple dynamical principles. Subsequently, the MC2's Navier-Stokes dynamics will transform that simple initial condition and adapt the quasi-straight flow to the terrain, within a few hours of physical time. All of the 162 runs use surface grids for the orography and land use.

Each simulation is performed as a dynamical downscaling of a quasi-geostrophic and horizontally uniform initial state. This is computationally less costly than the usual prognostic

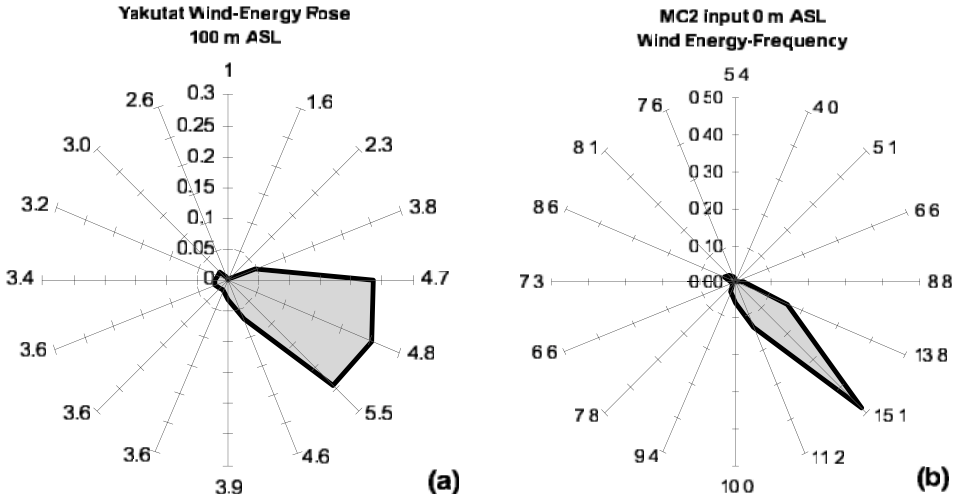

Fig. 6 Same wind energy-frequency roses as in the previous figure. The rose on the left is for the Yakutat upper air station at 100 m ASL and the one on the right is for the MC2 input at sea level. The MC2 input displays a sharper wind direction for the south-east than the Yakutat rose. The MC2 input wind speeds at sea level are also higher; they are considered as geostrophic, that is, without the effect of surface friction.

mode. The entire set of realizations is then combined according to the method of statistical-dynamical downscaling (Fuentes and Heimann, 1996). This results in a statistically rich set of two-dimensional (2-D) mesoscale numerical data, which consists of moments of the flow vectors from several low levels of the MC2, point wind rose frequency, kinetic energy flux; i.e., the so-called wind-power potential, joint speed-direction probability density function (PDF), and Weibull parameters of the joint PDF.

b *MC2 Input Climate Data versus Whitehorse and Yakutat Radiosonde Data*

To verify that the MC2 input climate data model is representative of the southern Yukon wind climate, it is compared to a forty-year time series of soundings from the Whitehorse upper air station at 1500, 3000, and 5500 m elevations and for the Yakutat upper air station at 100 m ASL. The Whitehorse station is well centralized in the model domain and should be representative of the regional wind climate. Yakutat is located in Alaska along the Pacific Coast and is 70 km to the south-west of Kluane National Park and 280 km west-south-west of Whitehorse. The soundings from the Whitehorse upper air station were compiled and arranged into the wind energy-frequency roses (explained in the next paragraph) shown in Figs 5a, 5c, and 5e. These roses are compared to those of the input data for MC2 which are in Figs 5b, 5d, and 5f. The Yakutat rose was compiled at 100 m ASL and is compared to the MC2 rose at level as shown in Fig. 6.

The orientation of the wind roses is such that north is towards the top of the page, east is the right arm, and so on. There are 16 sectors and each sector is 22.5° wide centred on the arm. The value at the end of each arm represents the long-term annual mean wind speed (m s^{-1}) in each direction sector. The perimeter of the area in the wind rose represents the wind energy-frequency in each direction. The wind energy-frequency is the percent frequency of wind occurrence multiplied by the cube of the mean wind speed and divided by the sum of those products in all directions.

The two wind datasets generally agree and show that there is a common trend of west to south-west winds at the levels above the mountaintops (at 3000 and 5500 m), and more south-easterly winds within the valleys (1500 m). At the 5500-m level, the MC2 input rose (Fig. 5b) displays a relatively stronger south-south-west component than the more widely south to west wind energy distribution of the Whitehorse rose (Fig. 5a). At this same level, the wind speeds (14 m s^{-1} from the south-west) for the Whitehorse radiosonde are about double those of the MC2 input (~7 m s^{-1} in the same general directions). At the 3000-m level, the Whitehorse rose (Fig. 5c) displays a narrower band of prevailing winds from the south-west than the level above, whereas the MC2 rose (Fig. 5d) displays a somewhat narrower south-south-west trend. The directional mean wind speeds of the MC2 input at 3000 m are weaker, being less than 70% of those for the radiosonde data.

The wind energy-frequency rose for the Whitehorse radiosonde station, shown at 1500 m in Fig. 5e, is typical of winds following the Whitehorse valley, which is in a north-north-west to south-south-east orientation. In the MC2 input data, the 1500-m level input, displayed in Fig. 5f, shows that the wind directions are more broadly spread with winds from the south to south-west. This broader distribution should be expected since it is not yet confined within any particular valley orientation when being applied to the model. The MC2 wind speeds are similar to those of the radiosonde at the same level except for the south-east arm where the wind speed is about 60% higher in the MC2 input.

The MC2 wind energy-frequency rose (Fig. 6b) at sea level reveals a strong south-east wind energy trend whereas Yakutat (Fig. 6a) is spread form the east to south-east. The model input winds at sea level seem rather high. The MC2

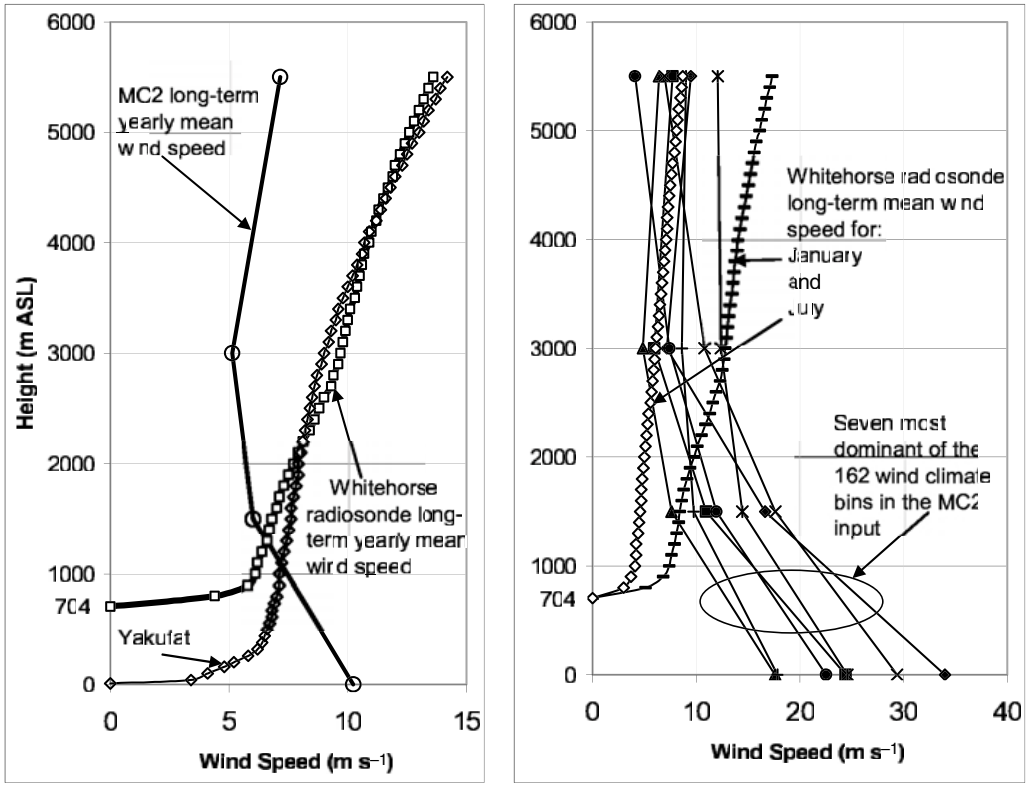

Fig. 7 The chart on the left shows an inverse relationship in the vertical profiles of long-term yearly mean horizontal wind speed between the MC2 input and the Whitehorse (704 m ASL) and Yakutat (10 m ASL) radiosonde data. We must keep in mind that the MC2 input wind speed is geostrophic. The chart on the right compares Whitehorse radiosonde profiles for January and July (15-year mean) with the seven dominant wind climate bins which represent 65% of the energy in the wind climate input data. The seven dominant wind bins are wind climates that occur in the wintertime. The comparison on the left shows that the MC2 input data tend to underestimate wind speeds at levels of 1500 m and up and overestimate them at sea level.

values are10–15 m s^{-1} compared to the Yakutat values of 4–6 m s^{-1}. One argument for the high wind speed at sea level is that it does not include surface effects (that is, it is geostrophic) and it should diminish when the model terrain is used.

Figure 7 shows more clearly the differences between the vertical profiles of the long-term mean wind speeds for the MC2 input and those of the Whitehorse and Yakutat radiosondes (15-year mean). The panel on the left shows that the average wind profile of the 162 climate bins of the MC2 input have a somewhat inverse relationship to the Whitehorse and Yakutat radiosonde profiles. The wind speeds for MC2 at 3000 to 5500 m are of the order of 5 m s^{-1} less than both the Whitehorse and Yakutat winds, which are 9 to 13 m s^{-1}. At the 1500-m level they are relatively close, between 6 to 8 m s^{-1}. The sea level mean input speed for MC2 is about 10 m s^{-1}, the highest mean wind speed in the MC2 profile. The Yakutat soundings show wind speeds of about 6 m s^{-1} at 300 m which then decline sharply to zero at the surface. In the panel on the right, the profiles for the seven dominant wind climate bins, which represent 65% of the total wind energy in the model, are shown along with the July and the January long-term mean wind speed from the Whitehorse radiosonde data. This panel is used for comparison with the panel on the left. The seven dominant bins occur in the winter but do not match the January profile for Whitehorse (they should be similar).

In Fig. 8 the potential temperature profiles of the seven dominant wind climate bins are shown along with the mean for all the climate bins. The figure also includes the 15-year January, July, and yearly means of potential temperatures from the Whitehorse radiosonde. The potential temperatures are converted from measured temperatures using a lapse rate of -1 K per 100 m rise in altitude starting at sea level. The yearly mean potential temperature profiles for the MC2 input and the radiosonde are very similar. They both show a quasi-linear rise in temperature from 283 K at 1000 m ASL to about 300 K at 5000 m. The seven dominant climate bin temperature profiles of the MC2 input are clustered around the values for the Whitehorse mean January radiosonde profile. This confirms that the seven dominant wind climate conditions should occur in the wintertime. Further analysis (not shown) indicates that the July profile for the radiosonde is at the upper temperature limit of the 162 wind climate bins.

A neutrally buoyant condition in Fig. 8 is a vertical line (i.e., potential temperature is height independent). As mentioned earlier, the temperature profiles at high latitudes reveal strongly stable atmospheric conditions throughout the year. This is evident here, where the mean potential temperature lapse rate of the MC2 input and the Whitehorse radiosonde average about +0.42 K/100 m. Strong stability suggests that the atmosphere is highly stratified, a condition in which the vertical

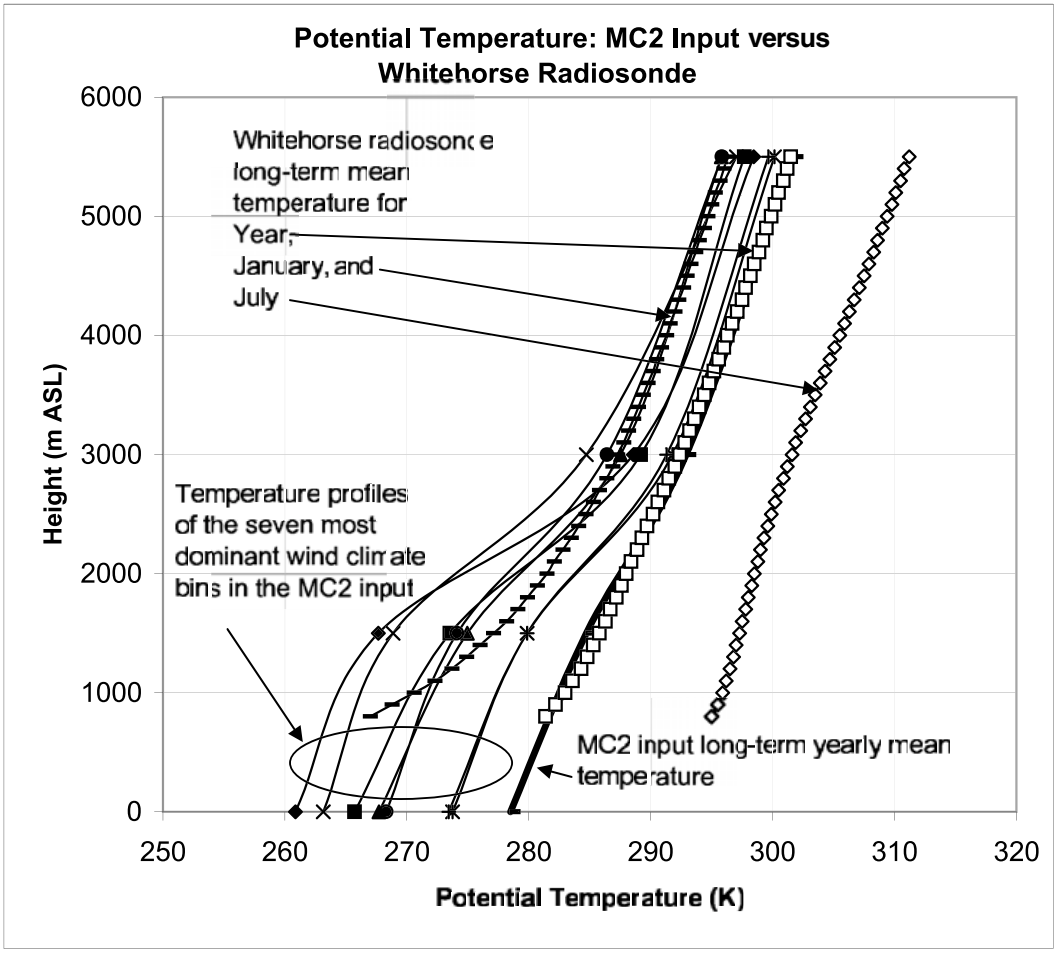

Fig. 8 Vertical profile of input potential temperature for the WEST simulation along with the Whitehorse radiosonde profile for (15-year mean) January, July, and year. The single thick line is the weighted mean potential temperature of all 162 climate categories. There is also a series of the seven most important wind climate bins which represent 65% of the wind energy of the whole bin set. The yearly mean temperature for both the Whitehorse radiosonde data and the MC2 input data are very similar in value. The series of seven are clustered around the Whitehorse January mean as expected as these seven bins occur in the winter.

mixing of the air from the mountaintop winds into the colder, denser valley air is less likely, especially in the winter.

c *The Surface Data*

Land use, or surface roughness, data are used by both the MC2 and the MS-Micro models to estimate winds near the ground. The roughness data used as input to WEST are based on vegetation classes identified by the United States Geological Survey (USGS) satellite classification. There are 26 roughness classes available for the WEST input and they are shown in Table 2. The land use map of the southern Yukon is accurate to 1 km and is represented in Fig. 9. This map shows that the territory is mostly covered by tundra, particularly at higher elevations. The valleys are dominated by boreal spruce (evergreen needleleaf) and poplar (deciduous broadleaf) forests. Other areas in between are covered by deciduous shrubs and lakes. In the south-west are the Kluane ice fields, an area dominated by ice as shown by the land use map. This ice may misrepresent the surface as being overly smooth, like a lake ice surface. The ice fields are generally covered by snow and may be rougher than a lake ice surface.

The land use values that coincide with the wind sites are shown in Table 3 and are compared with the observed land use and estimated values of surface roughness at each site. Overall, the surface is somewhat rougher than the land use data suggest. It should be noted here that the satellite data, which were likely acquired during the last decade, may not necessarily reflect the conditions at the airport sites that were monitored a few decades ago. The same is true for the field observations made more recently. The past surface conditions are not well known. There may have been buildings nearby, or the towers may have been moved. These possibilities cannot be excluded, although definite information has not come to light either from the literature or from conversations with knowledgeable locals. If the surface conditions were smoother (as pointed out in Section 3) then, this would imply that the wind speeds projected to 30 m would be less, thus widening the gap between the model output and the measured values, as will be seen later.

TABLE 2. The following are roughness classes used for interpreting the land use data in the satellite imagery. The map resulting from the assigned surface roughness, shown in Fig. 9, is used in MC2 and MS-Micro.

Roughness Class	z_o (m)	Surface description
1	0.001	water
2	0.001	ice
3	0.001	inland lake
4	1.5	evergreen needleleaf tree
5	3.5	evergreen broadleaf tree
6	1	deciduous needleleaf tree
7	2	deciduous broadleaf tree
8	3	tropical broadleaf tree
9	0.8	drought deciduous tree
10	0.05	evergreen broadleaf shrub
11	0.15	deciduous shrub
12	0.15	thorn shrub
13	0.02	short grass and forbs
14	0.08	long grass
15	0.08	arable
16	0.08	rice
17	0.35	sugar
18	0.25	maize
19	0.1	cotton
20	0.08	irrigated crop
21	1.35	urban
22	0.01	tundra
23	0.05	swamp
24	0.05	soil
25	1.5	mixed wood forest
26	0.05	transitional forest

The satellite land use data at 1-km resolution were applied to the 5-km grid of MC2. Those coincident grid-point values then represent larger areas, overriding the accuracy of the original data. Some land features may not be resolved faithfully on a 5-km square area. For example, the Teslin airport site was, according to the land use data, situated on water (z_o = 0.001 m) when in reality it was situated on land (z_o = 0.2 m).

The DEM data used in the MS-Micro simulations originate from 1:250,000 National Topographic Systems (NTS) from Canadian digital elevation data (NRCan, 2000) at Geomatics, Canada. The original DEM, spaced 93 m (north–south) by 35 to 65 m (east–west) is projected to a 333-m spaced microscale grid (see Fig. 2). The terrain grid used by MC2 is derived from the USGS 1-km DEM and is projected on the 5 km spaced mesoscale grid using area averaging (see Fig. 10). Figure 11 shows the elevation differences between the microscale and the mesoscale grids. The black areas in the figure show differences in elevations below -200 m. These areas are the original mountaintops that are being depressed through the conversion of a (relatively) real terrain to a 5-by-5 km spaced grid system. On the same grid, particularly where the land relief is more pronounced, such as along the Kluane Lake valley (Shakwak Trench), the mesoscale grid raises the land by over 200 m. These elevation changes in the mesoscale model are clearly noticeable by the elevation differences noted beside each site name in Fig. 11. The sites that are in the valleys are raised, on average, 230 m from their original elevations. The three mountaintop sites (Haeckel Hill, Paint Mountain, and Jubilee Mountain) are depressed by an average of 440 m.

The Bear Creek site, in a valley, is raised by 316 m from its real elevation of 670 m. The Kluane site is raised 352 m in the mesoscale terrain model from its original height of 786 m. The model grid point at Aishihik is approximately 1180 m high whereas the actual site is at an elevation of 966 m, raising the site by 214 m in the model terrain. The mountains to the south of the Aishihik station and just north of Paint Mountain are at mostly 1500 m with peaks above 2000 m, whereas in the model, the highest terrain is below 1400 m. The hills surrounding the valley of the Aishihik site are smoothed considerably. Paint Mountain is reduced by about 450 m from the actual station height of 1370 m. The mesoscale map topography shows that the grid point representing Paint Mountain is still relatively high compared to the surrounding terrain.

The Front Range that lies immediately south-west along Kluane Lake is not resolved; its peaks of 2500 m are "washed out" into a mere slope between the ice fields and Kluane Lake with an average height of about 1500 m in the mesoscale map. The isolated mountain at the south-east end of Kluane Lake has, in reality, a vertical relief of at least 1500 m and this is shown in the microscale map. In the mesoscale map this mountain barely exceeds 500 m in relief.

The differences between the site elevations as read from the NTS sheets and those of the microscale DEM are less dramatic. For the valley stations, there is a mean rise of only 26 m, and for the mountaintop sites, there is a mean drop of 67 m. In this same comparison the Haeckel Hill and Paint Mountain sites are prominent with elevation changes of about -134 and -176 m respectively.

d *The Grid Set-up and Simulations*

The MC2 mesoscale model domain covers a 500-km square portion of the southern Yukon. The grid has 151×151 points in the western and northern directions and each grid box is 5-km square in the horizontal direction. The domain becomes increasingly smooth beyond the 500-km model terrain, forming an "island" of a realistic Yukon topography in the middle of a flat plain. The DEM used for the MC2 simulation is shown in Fig. 10. The model's atmosphere is 20 km high and consists of 30 levels. Ten levels are below 1500 m, with the two lowest levels at 200 and 65 m above the surface.

The lateral boundaries of the MC2 model are open with inflow wind information being given at the four levels as described earlier; and the boundary values are time invariant. The upper and lower boundaries are solid. The lower boundary uses surface roughness information from the land use data. As indicated earlier, for the WEST simulations, most of the MC2 physics are inactive resulting in no surface radiation calculations but there is adiabatic boundary layer turbulent friction.

The MC2 model was run for each of the 162 wind climates for approximately nine hours of physical time. During each simulation the model terrain was initially flat and then increased to the full values over the first six hours. MC2 was set up in a time-independent mode and the remaining three

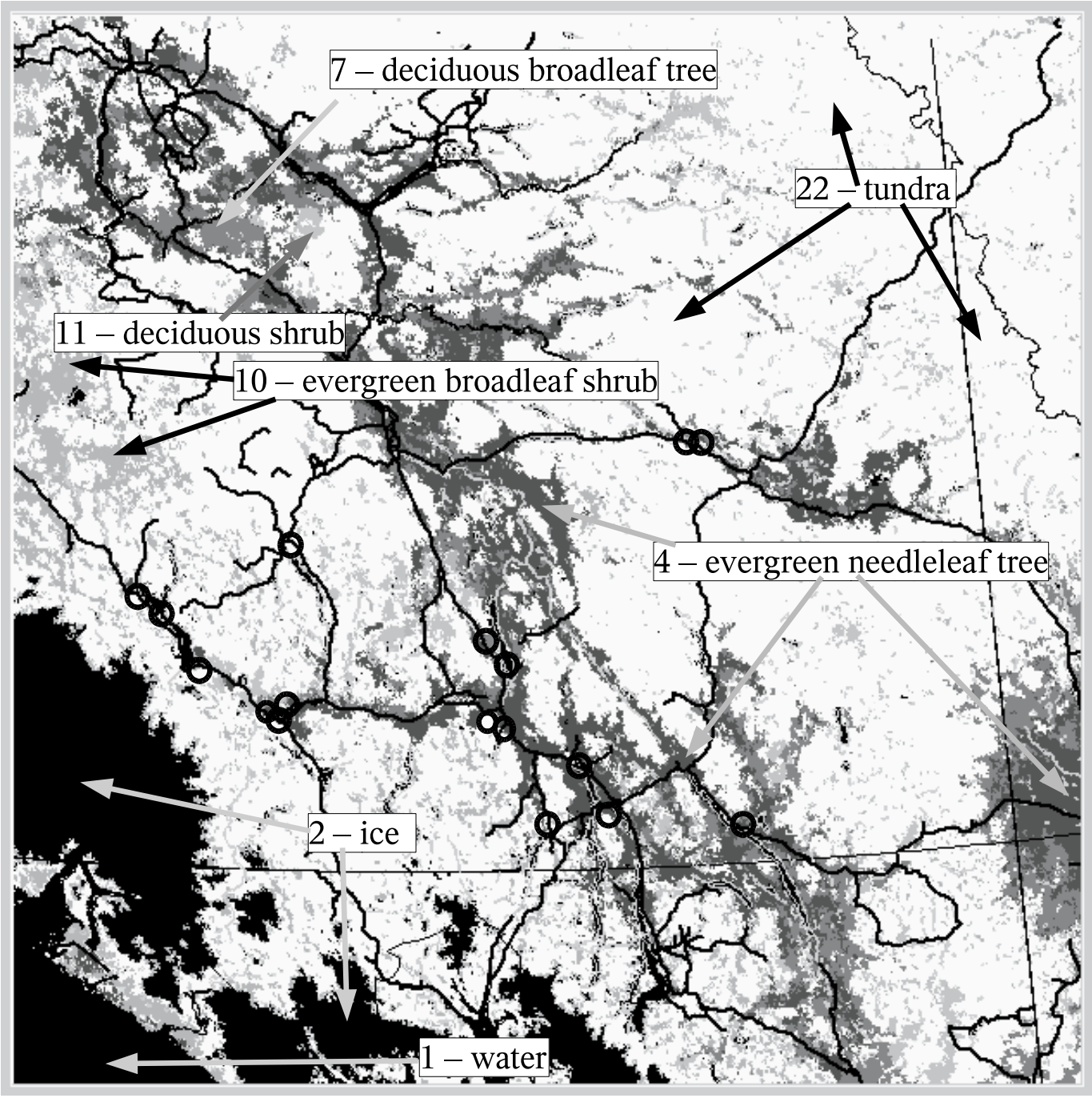

Fig. 9 Land use map of the southern Yukon can be referenced to Table 1 for the surface roughness values. This map shows that most of the southern Yukon is covered with tundra. The treed areas are typically located in the valleys. The areas indicated as ice are the Kluane ice fields, which are treated as having the same surface roughness as water.

hours were considered sufficient for the model to reach equilibrium. The output data for all 162 runs were compiled and made available for viewing and for input to MS-Micro.

The MS-Micro tiles have a full-width domain size of 42.5 km, with 128 points in the x and y directions (grid spacing is 333 m). The full-width domain includes a flat plain surrounding the model terrain. The horizontal size of the terrain is usually half the width of the whole domain. Each microscale domain is centred at every third grid point of the mesoscale domain, that is, every 15 km. Each domain overlaps its neighbour by a ratio of 0.3, normalized on the half-width. MS-Micro is run in several directions at each of the mesoscale grid points used by the microscale model. The joint frequency table of mean wind speed for each of the directions produced by MC2 is applied to the MS-Micro results. The resulting mean wind speed for each direction is then weight-averaged to one mean wind speed at a

TABLE 3. The land use data interpreted from the USGS satellite imagery is compared to the surface roughness observed and estimated in the field. The location of each station is identified on the satellite data interpretation map and the land use, surface roughness and vegetation description (referred to in Table 2) are extrapolated and shown in columns (2), (3), and (4). The observed surface roughness for each station was estimated by the first author through site visits and are listed in columns (5) and (6).

Column (1)	(2)	(3)	(4)	(5)	(6)
	According to satellite data interpretation			Observed in the field and estimated	
Wind Stations	Land use	z_o (m)	Vegetation type	z_o (m)	Vegetation type
Aishihik A	22	0.01	tundra	0.05	Open field with sparsely spaced shrubs
Burwash A	10	0.05	evergreen broadleaf shrub	0.1	Low-lying, field with nearby buildings and poplar
Faro A	22	0.01	tundra	0.1	Short grass field with nearby buildings and poplar
Haines Junction A	4	1.5	evergreen needleleaf tree	0.2	Low-lying field surrounded by spruce and buildings 200–500 m away
Kluane Lake A	10	0.05	evergreen broadleaf shrub	0.05	Open field with sparsely spaced shrubs
Teslin A	1	0.001	water	0.2	Short grass field with nearby buildings and poplar
Whitehorse A	6	1	deciduous needleleaf tree	0.02	Open field to the SE and NW.
Sheep Look-out, Faro	22	0.01	tundra	1	Poplar and spruce mix forest to 10-m heights
Haeckel Hill	22	0.01	tundra	0.01	Hill top tundra and short shrubs
Destruction Bay	22	0.01	tundra	0.05	Short grass, undulating surface on bank exposed to prevailing wind
Bear Creek	4	1.5	evergreen needleleaf tree	0.01	Open short grass field on bank exposed to prevailing wind
Fox Lake	4	1.5	evergreen needleleaf tree	3.85	Mature spruce forest to 15-m heights
Carcross	22	0.01	tundra	3.55	Poplar forest average 6-m heights
Lake Laberge	10	0.05	evergreen broadleaf shrub	0.01	Small rocky hill, by lakeshore and exposed to prevailing wind
Marsh Lake	1	0.001	water	0.01	Beach sand on lake shore, exposed to prevailing wind
Paint Mountain	4	1.5	evergreen needleleaf tree	0.05	Hill top tundra and short shrubs
Jubilee Mountain	22	0.01	tundra	0.05	Hill top tundra and short shrubs
	Mean z_o:	0.42	Mean z_o:	0.55	

given height for each microscale grid point. This averaged wind speed from MS-Micro is used for comparison with field measurements. The other statistics, such as the frequency and mean wind speed by direction, used for the wind rose comparisons, are obtained from the MC2 output. All microscale tiles are aggregated to produce a large microscale map covering the entire mesoscale domain. The DEM used for MS-Micro is shown in Fig. 2.

6 Results

The mean wind speed comparisons between the model and the field measurements are listed in Table 4. Here the stations are listed along with their elevations and tower heights in columns (2) and (3) respectively. Their mean wind speeds at, or projected to, 30 m are shown in column (4). Columns (5) and (6) show the model results from WEST (MC2 and MS-Micro) and from MC2 only. Column (7) shows the ratio of the WEST wind speeds to the measured wind speeds and column (8) shows the ratio of the MC2 wind speeds to the measurements. The WEST simulation generally predicts higher wind speeds than those observed. As shown by the mean ratios (bold font) in columns (7) and (8) in Table 4, the wind speeds of WEST and MC2 are approximately double those observed at the airport wind monitoring sites. The same WEST and MC2 simulations predict higher wind speeds at the wind energy stations by a factor of 1.4 and 1.2 respectively. The standard deviations of the ratios between the WEST and MC2 models and the measurements are lower for the wind energy stations, with values of 0.2 and 0.3 respectively, than for the values measured at the airport stations, 0.5 and 0.7 respectively. The model also correlates much better with the wind energy stations with $R = 0.95$ and 0.80 respectively than with the airport stations with $R = 0.49$ and 0.12 respectively.

The two groups of stations were originally treated as one until the graph in Fig. 12 revealed that there was (except for Whitehorse airport, Fox Lake, and Marsh Lake) a distinct difference between the wind speeds at the airport and the wind energy stations. A trend line is shown for each of those two groups; the grey line indicates agreement between the measurements and the model. Also shown on the graph are the total possible errors (vertical bars) due to vertical projection and period variability from long-term means. The error bars in Fig. 12 (also refer to Table 1 and Section 3) show that some stations such as Whitehorse, Carcross, and Lake Laberge may likely match the model output if the measurements actually underestimate the true wind speeds. In the graph in Fig. 12 it can be seen that the wind speeds from the WEST model agree best with the measurements from the Whitehorse airport and Haeckel Hill sites, giving higher speeds of about 10% (also refer to Table 4). For the rest of the wind energy sites the model predicts higher wind speeds than have been measured by 20 to 30% – except for the Marsh Lake and Fox Lake sites by 80 and 100% respectively. WEST predicts higher wind speeds for the airport group of stations by 70 to 170% (factor 1.7 to 2.7 times).

Further analysis concentrating on the Kluane region shows an isotach of the long-term annual mean wind speed at 30 m AGL resulting from the WEST simulation (Fig. 13). The map is overlaid with the locations of the wind monitoring sites along with their wind energy-frequency roses. As can be seen from the shaded areas on the isotach map, most of the stations

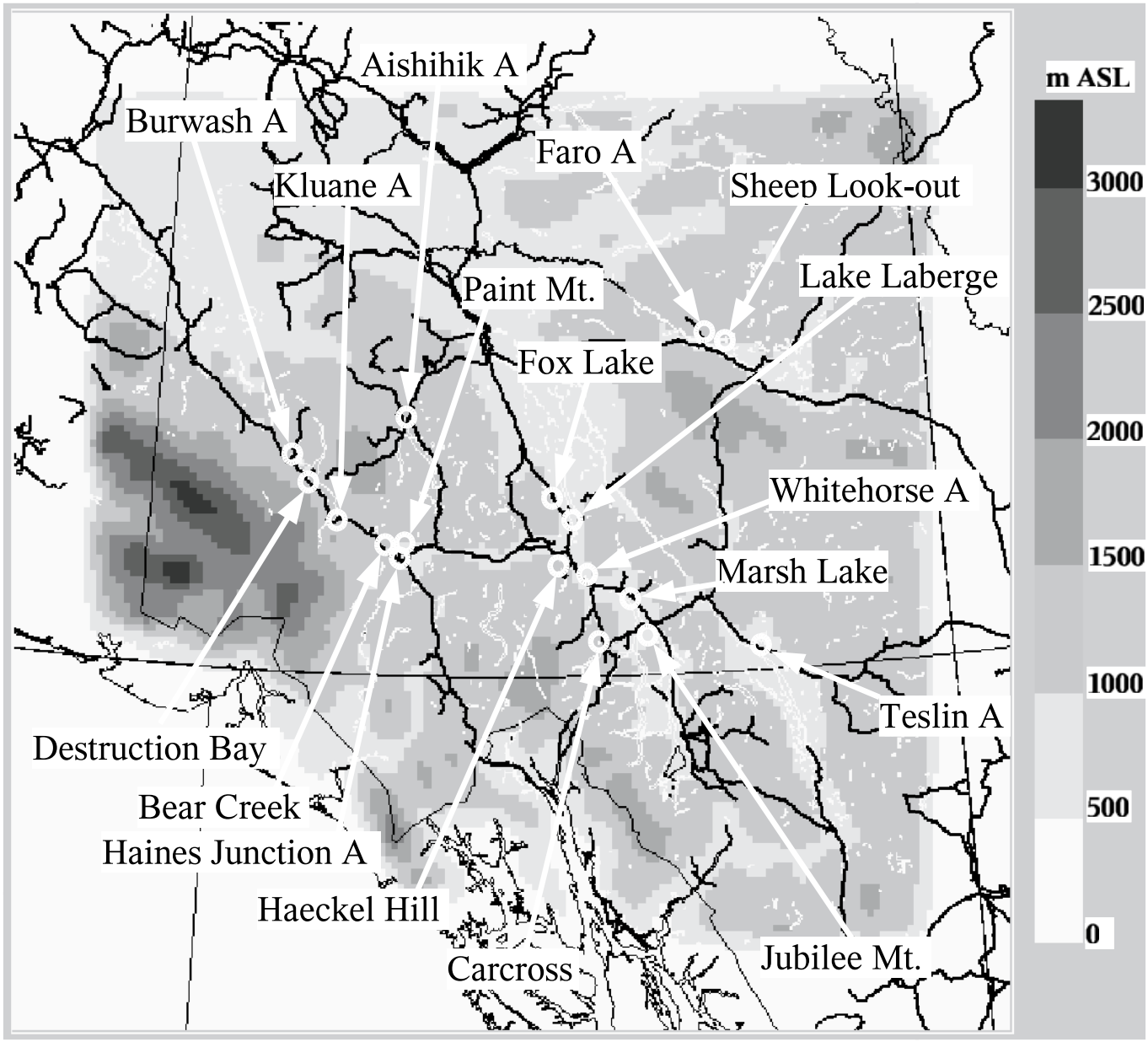

Fig. 10 The DEM used for the MC2 simulation. The 5-km spaced grid shows a less detailed terrain than the microscale map of Fig. 2. The mountainous features are smoothed out in this map.

in this region are predicted to have wind speeds in the 6 to 8 m s^{-1} range. The Aishihik airport site wind speeds are predicted to be 9 m s–1.

The wind energy-frequency roses for the measurements (light shading) at the Burwash airport and Destruction Bay sites show that more than 70% of the wind energy is from the east-south-east to south-south-east directions, following the valley axis. At the same two locations the model (dark shading) predicts a bimodal distribution for the direction of wind energy; one that is roughly from the south-east, and the other from the south-south-west. At the Burwash airport site, the dominant south-south-west to south-west energy component predicted by the model represents 60% of the total energy. This dominant wind direction is not supported by the measurements and a generally accepted belief that winds follow the valley axis. Despite the erroneous south-west modes, the MC2 model shows that the south-east modes of the Burwash airport and Destruction Bay sites agree with the directions of both station measurements. The model predicts 1.8 and 1.3 times higher wind speeds for the Burwash airport and Destruction Bay sites respectively.

The modelled rose for the Aishihik site in the north-east part of Fig. 13 compares very well with the measurements in terms of a southerly trend in direction. However, the wind speed comparison shows that the model simulates wind speed values which are 2.6 times the measured values. At Paint Mountain, the rose for the measured wind shows a small

TABLE 4. The following is a comparison of mean wind speeds between the model and the field measurements. The two groups, the airport and the wind energy stations, are shown along with their elevations in column (2). The measurement heights are in column (3) and the long-term mean annual wind speeds are in column (4). These measurements are projected to 30 m using Eq. (1) and the surface roughness information from the observed values in Table 3. Column (5) shows the results of long-term mean annual wind speed as modelled by MS-Micro from the output of MC2. Column (6) contains the values directly from MC2 projected to 30 m from 65 m AGL using Eq. (1) and surface roughness values from the satellite data shown in Table 2. The last two columns are ratios of the model results of WEST (MC2 and MS-Micro) and MC2 respectively divided by the measurements.

Column (1)	(2)	(3)	(4)	(5)	(6)	(7)	(8)
	Height	Field Measurement		WEST	MC2	Ratio	Ratio
	ASL (m)	Projected from (m)	30-m Speed (m s^{-1})	30-m Speed (m s^{-1})	30-m Speed (m s^{-1})	WEST/ Measured	MC2/ Measured
Airport							
Aishihik A	966	10	3.3	9.0	8.8	2.7	2.7
Burwash A	799	10	4.2	7.5	6.2	1.8	1.5
Faro A	694	10	2.7	5.6	5.9	2.1	2.2
Haines Junction A	599	10	2.3	5.3	5.6	2.3	2.5
Kluane Lake A	786	10	3.0	6.8	7.9	2.3	2.7
Teslin A	705	10	2.8	4.8	3.3	1.7	1.2
Whitehorse A	703	10	4.2	4.7	4.5	1.1	1.1
					Mean ratio model/field	**2.0**	**2.0**
					Standard Deviation	0.5	0.7
					Correlation (R):	0.49	0.12
Wind Energy							
Sheep Look-out, Faro	795	30	4.6	6.0	5.9	1.3	1.3
Haeckel Hill	1440	30	7.1	8.0	6.1	1.1	0.9
Destruction Bay	823	30	6.0	7.8	8.8	1.3	1.5
Bear Creek	670	26	5.0	6.4	5.3	1.3	1.1
Fox Lake	793	20	2.7	4.9	4.4	1.8	1.6
Carcross	702	20	4.1	4.8	4.8	1.2	1.2
Lake Laberge	645	10	4.5	5.6	4.9	1.3	1.1
Marsh Lake	656	10	3.0	5.4	3.9	1.8	1.3
Paint Mountain	1370	10	5.3	7.3	4.2	1.4	0.8
Jubilee Mountain	1280	10	4.3	5.9	4.1	1.4	1.0
					Mean ratio model/field	**1.4**	**1.2**
					Standard Deviation	0.2	0.3
					Correlation (R):	0.95	0.80

dominant east to south-east mode containing a little more than 40% of the wind energy and two smaller modes from the north-west and west-south-west. The model, on the other hand, predicts nearly 80% of the wind energy results from the south to south-west directions. MC2 predicts a lower wind speed at Paint Mountain by a factor of 0.8 but WEST predicts a higher wind speed by a factor of 1.4. The wind direction that the model predicts at Paint Mountain is similar to that of the Bear Creek site. At Bear Creek, the model predicts that almost 90% of the wind energy comes from the south to south-west, which is slightly more southerly compared to the measurements where about 95% of the wind energy comes from the south-west to west-south-west. MC2 predicts 10% higher wind speeds at the Bear Creek site, and WEST predicts 30% higher wind speeds.

The measured wind fields at the Kluane site showed three equally distributed modes in the south-west, south-east and north-west directions. At the same site, the model produced two modes similar to the Burwash airport and Destruction Bay sites. One mode has a more dominant component of 50% in the south-west and west-south-west directions and a smaller component in the south-south-east direction. Here the model more than doubles the wind speeds as measured at the Kluane site.

7 Discussion

The most important questions that arise in this study are why the WEST model predicts wind speeds which are 40% higher than the wind energy measurements and why there is a strong erroneous south-west wind component in the Kluane area.

One possible answer may lie in the mesoscale projection from the original DEM (the creation of a 5-km surface grid) which results in a smoothed topography. In the Kluane study area for example, nearly all of the stations in the mesoscale model are “lifted” (see Fig. 11) by at least 200 m in elevation. At the same time, some of the 2500-m peaks in the Front Range that lie immediately to the south-west, along Kluane Lake, become a simple 1500 m slope between the ice fields and Kluane Lake as a result of the smoothing. The flattening of the terrain relief is likely providing less orographic resistance and allowing strong winds into the raised valleys. The south-west wind component produced by the model in the Kluane Lake area, shown on the wind roses, results from flow through a non-existent Front Range.

The wind roses in Fig. 13 are overlaid on the mesoscale topography in Fig. 10 and are shown in Fig. 14, where it can be seen more clearly that the erroneous wind components modelled at each site in the Kluane region seem to point toward saddles in

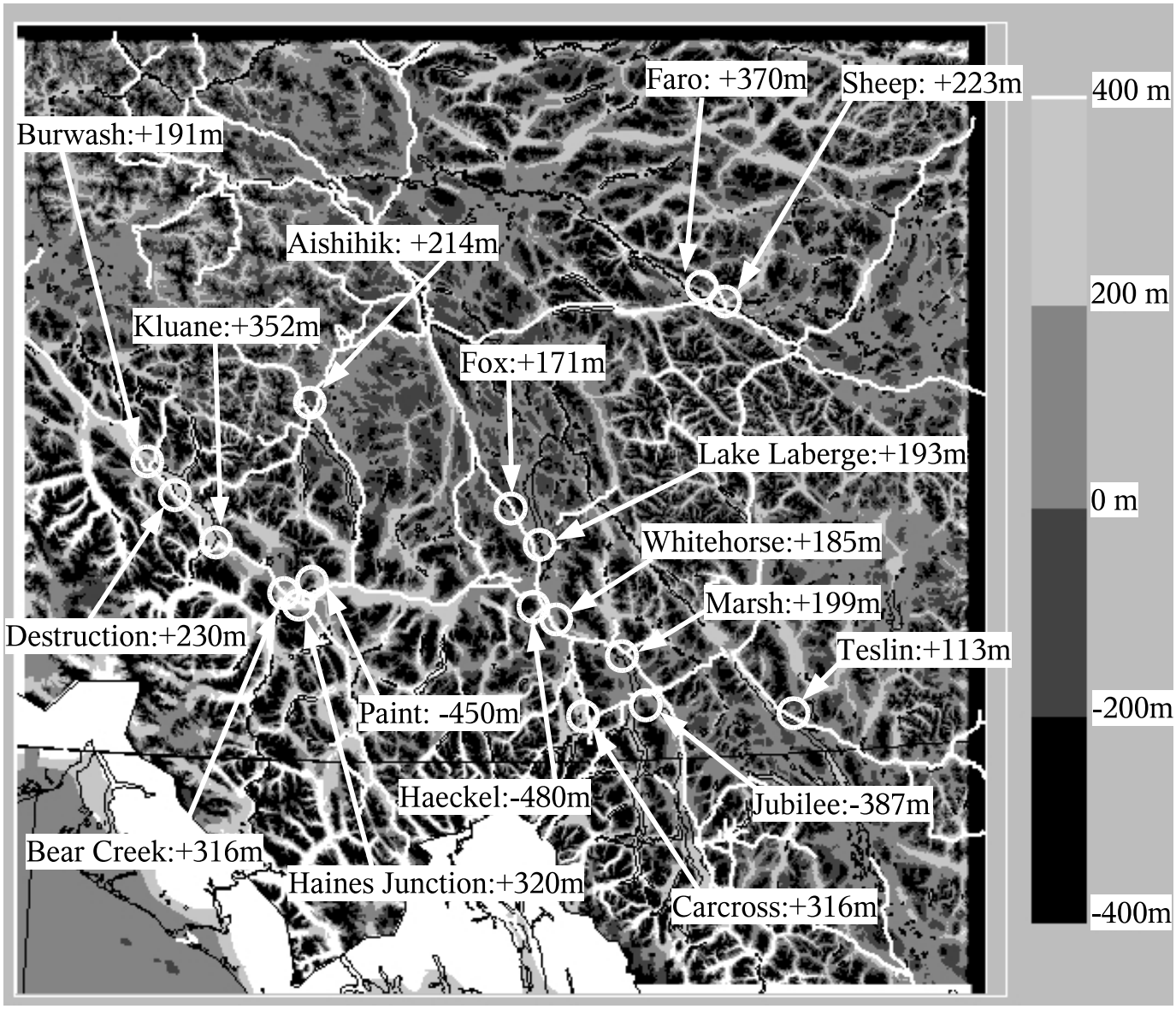

Fig. 11 An elevation map depicting the difference between the mesoscale and the microscale DEMs. The darkest areas represent a drop in elevation of at least 200 m where the mountaintops are normally located. The valleys tend to be uplifted. The elevation changes are more pronounced in locations such as the Kluane Lake area where the land is lifted up by more than 200 m in the mesoscale model.

the modified mesoscale terrain. At the Burwash, Destruction Bay, and Kluane Lake sites, those modes point towards a saddle on the east side of the St. Elias Mountains. At the Paint Mountain and Bear Creek sites, the modes point towards a much wider Alsek valley which is immediately to the south-west of these sites. It becomes evident that the terrain has been modified so much that wind regimes occur in the simulation which are not seen in the observations.

Another possible explanation for the high wind speeds around the Kluane region could be due to the smooth surface roughness assigned over the ice fields to the south-west of Kluane Lake (see lower left of Fig. 9). The ice field is given a roughness of z_o = 0.001 m which is equivalent to that of water or smooth flat ice. This smooth surface, along with a modified DEM, could allow for stronger winds to flow over the ice fields and onto the areas immediately to the north-east.

There are other factors relating to the land use that may have an adverse influence on the wind fields around the sites of interest. This can be more of a concern when modelling and measuring at low levels such as 10 m AGL. However, we have allowed for large errors in estimating the wind speeds to the standard height of 30 m AGL due to errant local surface roughness and atmospheric stability and we have allowed for errors due to the variability of a short wind monitoring period mean to represent a long-term mean.

The discrepancy in wind speeds between the MC2 and the MS-Micro outputs may be due to the use of every third point of the mesoscale grid in the MS-Micro simulations. A

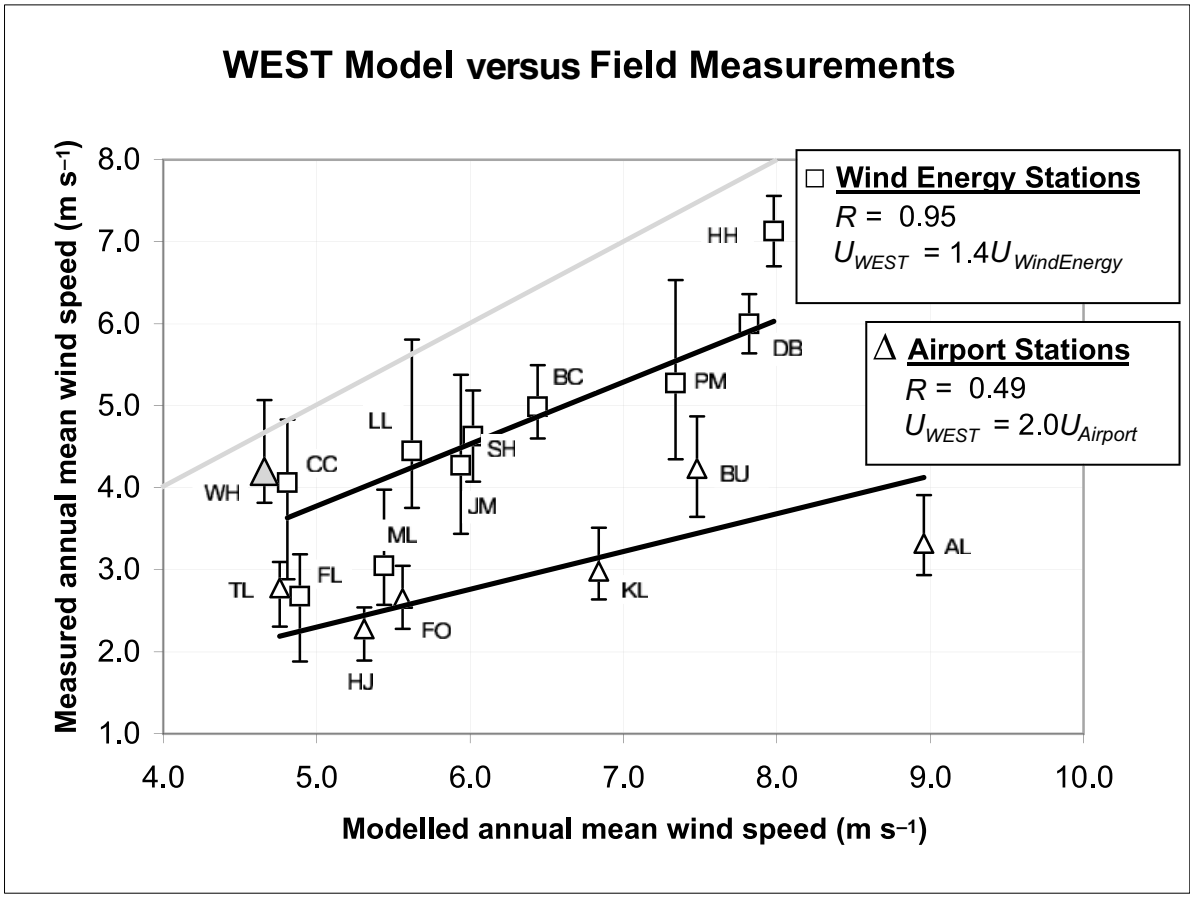

Fig. 12 A graphical comparison between the WEST simulation and the measurements from the airport and the wind energy stations. Trend lines are associated (Whitehorse not included) with each group. The grey line indicates where the model would ideally conform to the measurements. The vertical error bars represent the total error (see Table 1) due to vertical projection and to a shorter monitoring period of the wind speed measurements. The WEST simulation predicts better results at the wind energy stations than at the airport stations: WEST simulates 40% higher wind speeds at the wind energy stations, whereas, at the airport stations it simulates 200% (double) of the observed wind speeds. Despite the strong bias, the wind energy group shows a much stronger correlation with the model than the airport group. The symbols representing each station are as follows: AL – Aishihik Lake, BU – Burwash, FO – Faro, HJ – Haines Junction, KL – Kluane Lake, TL – Teslin, WH – Whitehorse, SH – Sheep Look-out, HH – Haeckel Hill, DB – Destruction Bay, BC – Bear Creek, FL – Fox Lake, CC – Carcross, LL – Lake Laberge, ML – Marsh Lake, PM – Paint Mountain, JM – Jubilee Mountain.

mesoscale grid point used as nearest neighbour to compare a site may not be the same point used for the MS-Micro simulations. Although computer resources and time are saved by using every third point for MS-Micro, perhaps concentrating the microscale runs to every grid point in areas of greater interest may be a better solution to this particular modelling problem.

The same concept of grid concentration mentioned above, could be applied at the mesoscale level, where in areas of greater interest, a finer grid could be nested within the main grid. In the Kluane Lake region, a finer grid of say 1 km would likely resolve the Front Range in a more satisfactory manner in the mesoscale terrain. The MS-Micro runs likely do not need to be applied to every grid point. If a selection procedure could be developed to choose the grid points in areas of interest where results are most important, then this would maximize the use of the computer resources. These areas of interest are usually within a few tens of kilometres from power lines and communities.

It is possible that the high input wind speed at sea level may contribute to simulated wind speeds which are too strong. The elevation in the mesoscale model is mostly 1000 m ASL and should cause the sea level winds to flow around the model topographical “island”. This effect would need to be studied through a detailed look at a vertical profile of the wind roses around the island.

A possible problem that might be of concern in WEST is in some of the limitations of MS-Micro. MS-Micro is only capable of modelling terrain that has slopes of less than about one in four. While the mountains generally are within that limitation there are areas that are steeper. At most sites of interest, however, the mountain slopes seem to be within this limitation. In most cases, those mountains that exceed the slope limitation are not accessible for wind development. But at Destruction Bay, for example, the site is relatively close to the edge of an escarpment that has a slope of about one in two. Since the model grid is already quite coarse at 333 m, a

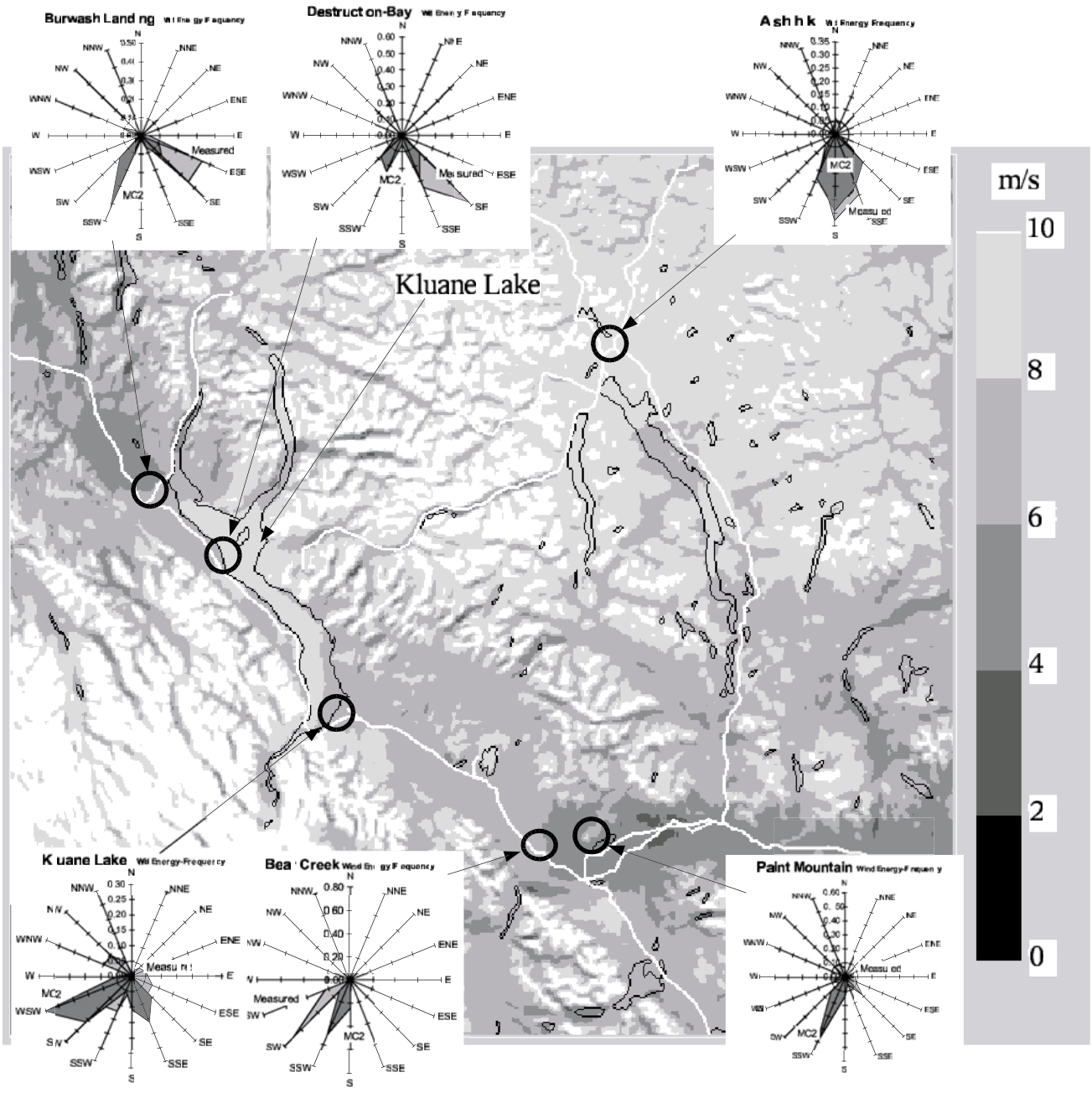

Fig. 13 An isotach map of 30-m (AGL) long-term annual mean wind speed as produced by WEST for the Kluane region. The map is overlain by the sites of the monitoring stations along with wind energy-frequency roses for both the field measurements and the model. The roses representing the measurements are in a lighter shade and are overlapped by the MC2 output in the darker shade. For all of the stations in this region, except for Aishihik airport at 9 m s^{-1}, the WEST model predicts their wind speeds to be in the 6 to 8 m s^{-1} range.

sudden elevation of about 40 m is smoothed to a very slight slope of about one in eight.

Another limitation in MS-Micro that could be a source of error, is the assumption of neutral stability. The neutral assumption implies a smaller wind shear; hence, a narrower vertical profile of horizontal wind speeds. Since wind speed inputs to MS-Micro are from higher levels such as 65 m AGL, this likely causes MS-Micro to predict higher wind speeds at lower levels. This also raises the question as to whether these stable atmospheric conditions are properly simulated in the MC2 model. The turbulence closure scheme in MC2 is designed to account for temperature profiles by means of a static stability function that is dependant on the Richardson number. In a future analysis it may be useful to produce outputs of vertical profiles of wind speed and temperatures to verify that this stability effect is occurring and properly influencing the simulated wind flows in the model. If the stability effect were accounted for in MS-Micro, as is apparently the case in MC2, then this effect should

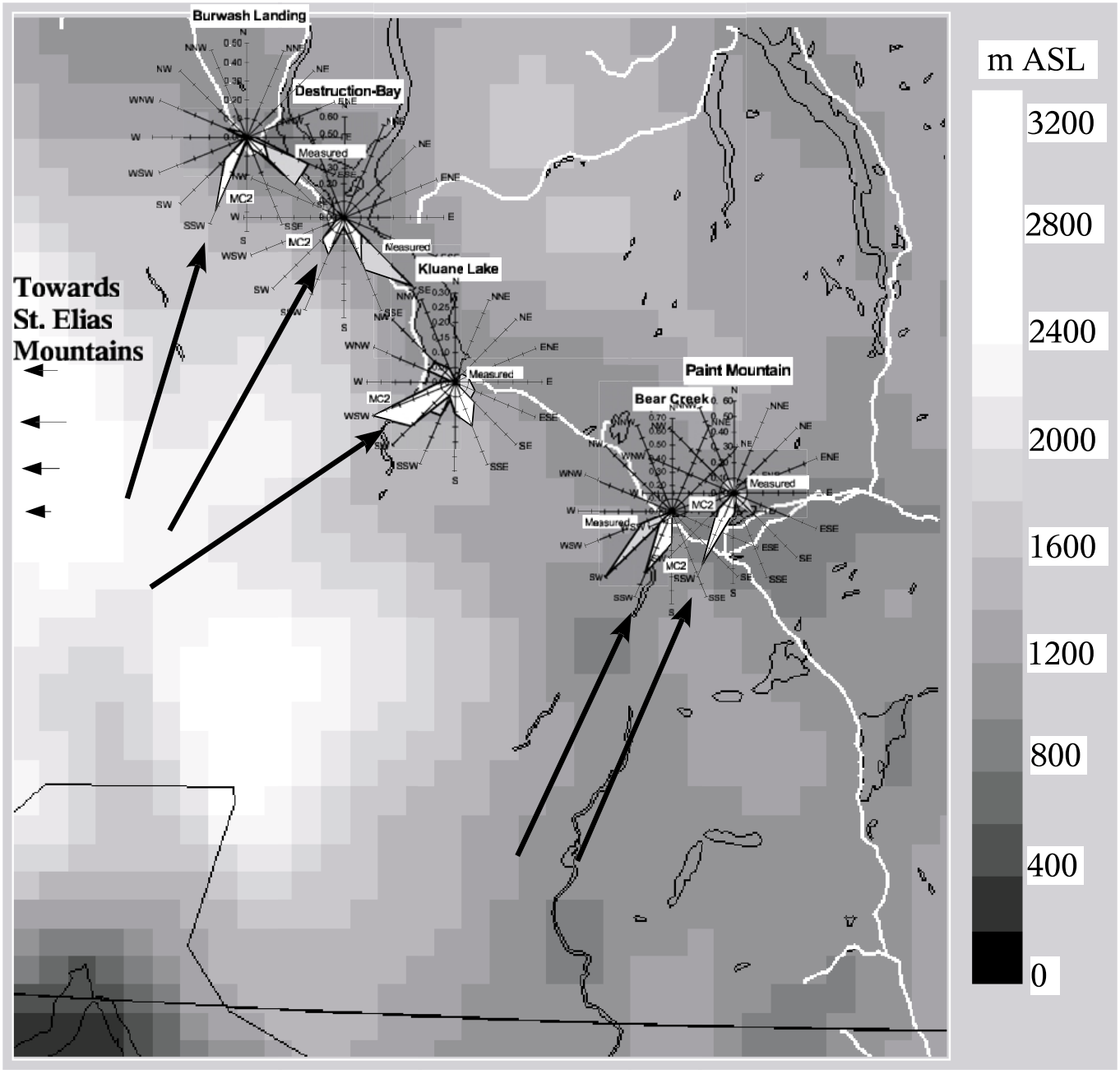

Fig. 14 Wind energy-frequency roses overlain on the 5-km spaced mesoscale surface elevation grid of the same Kluane region shown in Fig. 13. Roses from the model results are white and those from the measurements are grey. The heights labelled in the legend are in metres ASL. The black arrows illustrate some of the wind directions from which the model predicts at each of the five sites.

increase the wind shear, thus reducing the wind speed near the ground in the WEST simulation.

It is interesting to note the difference in the trends between the wind energy stations and the airport stations when comparing them to each other via the WEST simulations. Assuming that the wind energy group is the more correct one, and that the WEST simulation is accurate (although highly biased), the airport group then seems to underestimate wind speeds to about 60% (MC2 only) or 70% (WEST). It is not certain why there seems to be an underestimation by the airport stations but two possible reasons are suggested. The method for measuring wind speed on the hour by reading from a dial and recording on paper is prone to human error and could possibly underestimate the true wind speed. This underestimation could be larger for those airport sites which take observations only during office hours. The other reason is that the airports, and their accompanying stations are typically "not" located in areas of high wind speed conditions, perhaps for safety reasons with regard to the landing of aircraft.

8 Conclusions

The mean annual wind speeds from ten wind energy stations are higher than the measured annual wind speeds predicted by

the WEST model, which couples MC2 and MS-Micro, by about 40%. However, the correlation coefficient between the series of long-term mean wind speeds for the model and the wind energy stations is high, with a value of $R = 0.95$. The predicted wind speeds from the MC2 model used alone are only 20% higher than those measured at the wind energy stations.

The measured wind speeds at seven airport weather stations also used in the model comparison are approximately half of the wind speeds predicted by the model. The airport stations also have a poor correlation coefficient of $R = 0.49$ with the model. Interestingly, with the WEST simulation, most of the airport stations seem to measure wind speeds that are roughly 60 to 70% that of the wind energy stations. This discrepancy might result from airport stations being located in relatively sheltered areas and to the method in which wind data were measured and collected.

An examination of the wind roses for both the wind stations and the model output in the Kluane Lake region reveals some agreement with the measured wind directions following the valley orientations. Along Kluane Lake, however, the model shows erroneous wind directions that are nearly perpendicular to the valley axis. The odd wind directions and strong wind speeds simulated by WEST may be most influenced by a modified and somewhat flattened terrain in the mesoscale elevation model. It is illustrated that in the Kluane region the erroneous directions seem to point to simulated winds flowing over saddles or passes through modified terrain east of the St. Elias Mountains.

Other possible influences on the biased wind speeds in the model could be attributed to the following:

1. Raised valleys and lowered mountains in the mesoscale terrain may increase simulated wind speeds in the valleys. The 5-km mesoscale grid may perhaps be overly modified during the conversion process. It would be useful to investigate the conversion process to find ways to reduce discrepancies between the original and the mesoscale terrain. This process may also be applicable to the microscale terrain.
2. The assumption of neutral stability in MS-Micro may likely lead to predicted higher wind speeds in the model. Vertical wind shears in the more stable atmospheric conditions of the Yukon are higher, resulting in lower wind speeds near the ground relative to the winds above. This phenomenon needs to be verified in the MC2 model.
3. The general application of MS-Micro to every third mesoscale grid point may be the cause of the deterioration of the MS-Micro wind speed results relative to MC2. If computer resources are a problem then it may be useful to allow the possibility that the microscale model can be applied to the nearest grid point of a wind site of interest.
4. Abnormally high sea level (geostrophic) wind speeds in the MC2 wind climate input may create high near-surface wind speeds in the MC2 simulations. This may or may not be an issue because the terrain in the model is raised to over 1000 m ASL and these sea level winds may be reduced by the terrain surface drag and diverged around the “island”. It would be useful, however, to study vertical profiles and wind roses throughout the model atmosphere to determine the influence of the input wind speed used in the MC2 simulation.
5. Mismatched land use at the model surface may cause errant wind speeds near the surface. In areas such as the Kluane ice fields, the smooth surface roughness may allow higher wind speeds over this area.

The WEST is a promising candidate for providing solutions of the wind fields near the surface in the mountainous regions of the Yukon. However, the points noted above need to be investigated further to improve the model. The modified mesoscale terrain, in particular, needs the most attention. Any improvement in the grid’s ability to represent the original terrain may provide the biggest improvement in the model’s ability to simulate winds in mountainous terrain such as that of the Yukon.

Acknowledgments

The data used in this study is owned by and copyrighted to Yukon Energy and the Yukon Development Corporation. Permission has been granted by both aforementioned owners to use these data to carry out the comparative study. Acknowledgement is also given to Environment Canada, to John D. Wilson of the University of Alberta and to Bill Miller of Environment Canada in Whitehorse for the helpful information about the airport stations.

References

ADRIAN, G. and F. FIEDLER. 1991. Simulation of unstationary wind and temperature fields over complex terrain and comparison with observations. *Contrib. Atmos. Phys.* **64**: 27–48.

AES. 1976. Climatological station data catalogue. Technical report, Environment Canada, Downsview, Ontario, 34 pp.

——. 1982. Canadian Climate Normals Vol. 5 1951–1980. Technical Report, Environment Canada, 283 pp.

BAKER, D. R. 1995. Annual report wind monitoring and analysis. Technical report, Nor’wester Energy Systems Ltd., for Yukon Energy Corporation, 350 pp.

BENOIT, R.; M. DESGAGNE, P. PELLERIN, S. PELLERIN, Y. CHARTIER and S. DESJARDINS. 1997. The Canadian MC2: A semi-Lagrangian, semi-implicit wideband atmospheric model suited for finescale process studies and simulation. *Mon. Weather Rev.* **125**: 2382–2415.

——; W. YU and D. LEMARQUIS. 2001. Mesoscale mapping of the wind energy climate of Canada. *In*: Proc. CANWEA 2001 Annual Conference, 25 pp.

BROWER, M.; J. W. ZACK, B. BAILEY, M. N. SCHWARTZ and D. L. ELLIOT. 2004. Mesoscale modeling as a tool for wind resource assessment and mapping. *In*: Proc. 14th Conf. on Applied Climatology, Am. Meteorol. Soc., available at http:// ams.confex.com.

COTTRELL-TRIBES, C. 2000a. Destruction Bay wind analysis. Technical report, Yukon Energy Corporation, John Maissan (Ed.), 11 pp.

——. 2000b. Haeckel Hill wind analysis: December 1998 to October 1999. Technical report, Yukon Energy Corporation, John Maissan (Ed.), 26 pp.

——. 2001. Phillips wind analysis: August 2000 - July 2001. Technical report, Yukon Energy Corporation, John Maissan (Ed.), 6 pp.

——. 2002a. Abbot wind analysis: August 2001 - July 2002. Technical report, Yukon Energy Corporation, John Maissan (Ed.), 43 pp.

——. 2002b. Lendrum wind analysis: August 2001 - July 2002. Technical report, Yukon Energy Corporation, John Maissan (Ed.), 24 pp.

——. 2002c. Luet wind analysis: August 2001 - July 2002. Technical report, Yukon Energy Corporation, John Maissan (Ed.), 41 pp.

——. 2003. Faro sheep site wind analysis: August 2000 to June 2002. Technical report, Yukon Energy Corporation, John Maissan (Ed.), 295 pp.

ELLIOTT, D. and M. SCHWARTZ. 1993. Wind energy potential in the United States. PNL-SA-23109, Pacific Northwest Laboratory, available at www.nrel.gov.

FRANK, H. P. and L. LANDBERG. 1997. Modelling the wind climate of Ireland. *Boundary Layer Meteorol.* **85**: 359–378.

——; E. L. PETERSEN, R. HYVONEN and B. TAMMELIN. 1999. Calculations on the wind climate in northern Finland: the importance of inversions and roughness variations during the seasons. *Wind Energy*, **2**: 113–123.

FUENTES, U. and D. HEIMANN. 1996. Verification of statistical-dynamical downscaling in the alpine region. *Climate Res.* **7**: 151–168.

JACKSON, P. S. and J. C. R. HUNT. 1975. Turbulent wind flow over a low hill. *Q. J. R. Meteorol. Soc.* **101**: 929–955.

KALNAY, E.; M. KANAMITSU, R. KISTLER, W. COLLINS, D. DEAVEN, L. GANDIN, M. IREDELL, S. SAHA, G. WHITE, J.WOOLLEN, Y. ZHU, A. LEETMAA, R. REYNOLDS, M. CHELLIAH, W. EBISUZAKI, W. HIGGINS, J. JANOWIAK, K. C. MO, C. ROPELEWSKI, J. WANG, R. JENNE and D. JOSEPH. 1996. The NCEP/NCAR 40-year reananlysis project. *Bull. Am. Meteorol. Soc.* **77**: 437–471.

MAILHOT, J.; S. BELAIR, R. BENOIT, B. BILODEAU, Y. DELAGE, L. FILLION, L. GARAND, C. GIRARD and A. TREMBLAY. 1998. Scientific description of RPN physics library - version 3.6. Technical report, Recherche en Prévision Numérique, Meteorological Service of Canada, 197 pp.

MASON, P. J. and R. I. SYKES. 1979. Flow over an isolated hill of moderate slope. *Q. J. R. Meteoral. Soc.* **105**: 383–395.

MORTENSEN, N.; L. LANDBERG, I. TROEN and E. PETERSEN. 1993. Wind Atlas Analysis and Application Program (WAsP). Technical Report Riso National Laboratory, 172 pp.

NATIONAL GEOGRAPHIC. 2002. Power till the cows come home – mapping Canada's winds help promote an underused energy resource. 2 pp.

NRCAN. 2000. Canadian digital elevation data - standards and specifications. Technical report, Natural Resources Canada, Geomatics Canada, Centre for Topographic Information Customer Support Group 2144 King St. West, Suite 010 Sherbrooke (Québec) J1J 2E8, available online at www.cits.nrcan.gc.ca.

PINARD, J. D. J. 2001. Yukon wind energy potential, Bear Creek wind monitoring study. Technical report, Boreal Alternate Energy Centre, prepared for the Community Development Fund, Yukon Territorial Government, 16 pp.

TANGUAY, M.; A. ROBERT and R. LAPRISE. 1990. A semi-implicit semi-Lagrangian fully compressible regional forecast model. *Mon. Weather Rev.* **118**, 1970–1980.

TAYLOR, P. A.; J. L. WALMSLEY and J. R. SALMON. 1983. A simple model of neutrally-stratified boundary-layer flow over real terrain incorporation wavenumber-dependent scaling. *Boundary-Layer Meteorol.* **26**: 169–189.

TROEN, I. and E. L. PETERSEN. 1989. *European Wind Atlas*. Riso National Laboratory, Roskilde, Denmark, for the Commission of the European Communities ISBN 87-550-1482-8, 656 pp.

VINCENT, M. 2001. Who has mapped the wind? Canadian Geographic, 2 pp.

WALMSLEY, J. L.; J. R. SALMON and P. A. TAYLOR. 1982. On the application of a model of boundary layer flow over low hills to real terrain. *Boundary-Layer Meteorol.* **23**: 17–46.

——; P. TAYLOR and T. KEITH. 1986. A simple model of neutrally stratified boundary-layer flow over complex terrain with surface roughness modulations (MS3DJH/3R). *Boundary-Layer Meteorol.* **36**: 157–186.

——; WOOLRIDGE and J. SALMON. 1990. MS-Micro/3 user's guide. Technical Report. ARD-90-008, Atmospheric Environment Service, 85 pp.

—— and R. J. MORRIS. 1992. Wind energy resource maps for Canada. Technical report, Atmospheric Environment Service, 53 pp.

WSD. 1977. MANOBS - manual of surface weather observations. Technical report, Weather Services Directorate, Environment Canada, pp. 7-1–7-7.